Publisher: GSA
Journal: GEOL: Geology
DOI:10.1130/G38363.1

The cause of Late Cretaceous cooling: A multi-model/proxy comparison

Clay R. Tabor[1,2], Christopher J. Poulsen[1], Daniel J. Lunt[3], Nan A. Rosenbloom[2], Bette L. Otto-Bliesner[2], Paul J. Markwick[4], Esther C. Brady[2], Alexander Farnsworth[3], and Ran Feng[2]

[1]Department of Earth and Environmental Sciences, University of Michigan, 2534 C.C. Little Building, 1100 North University Avenue, Ann Arbor, Michigan 48109, USA

[2]National Center for Atmospheric Research, 1850 Table Mesa Drive, Boulder, Colorado 80305, USA

[3]School of Geographic Sciences, University of Bristol, University Road, Clifton, Bristol BS8 1SS, UK

[4]Getech, Kitson House, Elmete Hall, Elmete Lane, Leeds, LS8 2LJ, UK

ABSTRACT

Proxy temperature reconstructions indicate a dramatic cooling from the Cenomanian to Maastrichtian. Yet the spatial extent of and mechanisms responsible for this cooling remain uncertain given simultaneous climatic influences of tectonic and greenhouse gas changes through the Late Cretaceous. Here, we compare several climate simulations of the Cretaceous using two different Earth System models with a compilation of sea-surface temperature proxies from the Cenomanian and Maastrichtian, to better understand Late Cretaceous climate change. In general, surface temperature responses are consistent between models, lending confidence to our findings. Our comparison of proxies and models confirms that Late Cretaceous cooling was a

widespread phenomenon and likely due to a reduction in greenhouse gas concentrations in excess of a halving of CO_2, not changes in paleogeography.

INTRODUCTION

The Cretaceous is often characterized as a greenhouse climate with CO_2 concentrations in the realm of IPCC business-as-usual estimates for 2100 (Wang et al., 2014). Despite general warmth, evidence suggests significant climate changes occurred during this period. Across the Late Cretaceous (101–66 Ma), proxy temperature reconstructions indicate a cooling trend from the Cenomanian/Turonian Thermal Maximum to the Maastrichtian (Huber et al., 2002; Pucéat et al., 2007; Friedrich et al., 2012; Linnert et al., 2014). Both temporally (Huber et al., 2002; Pucéat et al., 2007) and spatially discreet (Linnert et al., 2014) sea-surface temperature (SST) reconstructions suggest several degrees of cooling from 101 to 66 Ma, though some disagreements about the latitudinal temperature gradient response exist (Pucéat et al., 2007). This cooling occurred in concert with large-scale tectonic changes such as restriction of the Arctic ocean and expansion of the Atlantic ocean (e.g., Sewall et al., 2007), a reduction in atmospheric CO_2 (e.g., Wang et al., 2014), and the radiation of angiosperms (e.g., Boyce et al., 2009), which makes determining the cause of Late Cretaceous climatic change uncertain. A dearth of long-term temperature records (Linnert et al., 2014) and consistent climate simulations spanning the Late Cretaceous (Donnadieu et al., 2006) exacerbate the problem.

To better understand the mechanisms responsible for the Late Cretaceous cooling, we compare several Earth System model simulations with a compilation of SST proxies from the Cenomanian (CEN) (100.5–93.9 Ma) and Maastrichtian (MAA) (72.1–66.0

Ma). We chose these stages because they represent temporal and climatological end-members of the Late Cretaceous and have small across-stage temperature trends compared to other stages within the period (Friedrich et al., 2012). Our model simulations allow us to separate the Late Cretaceous temperature responses due to changes in geography from responses due to reduction in CO_2. These simulations, in combination with our SST proxy compilation, provide insight into the extent, magnitude, and mechanisms responsible for the Late Cretaceous cooling.

METHODS

Climate Simulations

We use the Community Climate System Model (CCSM4) and Hadley Centre Model (HadCM3L) with identical paleogeographies, greenhouse gas (GHG) concentrations, total solar irradiance (TSI), and orbital configurations. Both models contain dynamic atmosphere, ocean, sea ice, land surface, and vegetation components. Here, CCSM4 has a 1.9x2.5° atmosphere/land-surface grid and ~1° ocean/sea-ice grid, and HadCM3L has a 2.5x3.75° grid for all model components. These models have been previously used for several paleoclimate simulations (e.g., Rosenbloom et al., 2013; Lunt et al., 2016).

We use 0.5° global topography and bathymetry reconstructions created by Getech Plc (http://www.getech.com/globe/), using similar methodologies to those presented in Markwick and Valdes (2004). In this study, we focus on paleogeographic reconstructions of the CEN and MAA (Fig. DR1). All experiments use age appropriate TSI (Gough, 1981) with a present-day orbital configuration. CO_2 concentrations are set to either 4x or

2x preindustrial (PI) (1120 or 560 ppm), roughly representative of proxy-reconstructed averages across the Late Cretaceous (Wang et al., 2014).

We run all CCSM4 simulations for 1500 years and all HadCM3L simulations for 1422 years, long enough for the upper ocean (100 m) and atmosphere to reach near-equilibrium. All results are climatologies from the final 30-years of the model runs. Below we explore three model configurations with both CCSM4 and HadCM3L: a 4x PI CO_2 CEN case (CEN4x), a 4x PI CO_2 MAA case (MAA4x), and a 2x PI CO_2 MAA case (MAA2x).

Proxy Records

SST proxy records come from a combination of planktonic foraminifera (PF), fish tooth enamel, shells of mollusks, bivalves, brachiopods, and belemnite rosta, and TEX_{86}. Proxy values represent data averages of studies from the CEN and MAA based on published ages, with averaging done over the entire age and for nearby sample locations from a single study and technique. To allow for a more direct comparison, we use several standard SST calibrations. Here, we only provide analytical and/or calibration uncertainties, which represents a minimum estimate of proxy uncertainty range over an age. To correct seawater $\delta^{18}O$ ($\delta^{18}O_{sw}$) for regional variability, we use model stage-specific salinity (Poulsen et al., 1999) with the relationship of Broecker (1989) and assume a mean $\delta^{18}O_{sw}$ of −1‰ Vienna Mean Standard Ocean Water (VSMOW) (Shackleton and Kennett, 1975). See Data Repository for additional methodology.

RESULTS

Model Results

Both models produce similar global-mean surface temperature (TS) for all CEN and MAA experiments (Table DR1, Figure 1a-c,g-i, DR2). On average, CCSM4 is warmer than HadCM3L by 0.67 °C, mainly due to slightly higher SSTs. The largest difference occurs in the high-latitudes of the South Pacific where CCSM4 TS is up to 10 °C warmer due to greater ocean heat transport into the region and less cloud cover (Fig. 1a-f, DR2, DR3). In contrast, CCSM4 land-surface temperatures (LST) tend to be cooler than HadCM3L. Much of these difference stems from model vegetation. In low latitudes, greater evapotranspiration in CCSM4 leads to more latent heat release (Boyce et al., 2009), while at high latitudes, less vegetation in CCSM4 reduces canopy masking of snow-cover and raises surface albedo (Fig. DR4). Regardless of regional differences, both models tend to agree on the sign and magnitude of TS change with changes in paleogeography and CO_2, particularly in the low to mid-latitudes where proxy density is greatest (Fig. 1 g-i, DR2, DR5, DR6).

Response to Paleogeography

Changes in geography and TSI from CEN4x to MAA4x lead to minor global-mean TS responses with only 0.14 °C of warming, almost completely in response to a 3.28 Wm^{-2} increase in solar constant across the Late Cretaceous (Fig. DR6a,b). This is mirrored by minimal temperature changes from CEN4x to MAA4x associated with global average emissivity (0.13 °C), albedo (−0.16 °C), and heat transport (0.00 °C) with no change greater than 0.24 °C for either model based on our model energy balance calculations (see Data Repository). Nevertheless, robust regional temperature changes exist from CEN4x to MAA4x. For instance, the North Pacific warms in both models, likely due to a reduction in cloud cover (Fig. DR3) and the closure of the Bering Strait, which allows less mixing with cold Arctic water. Eastern North America, however, experiences widespread cooling due to reduced warm inflow from the gulf with the closure of the Western Interior Seaway in the latest Cretaceous (Poulsen et al., 1999) (Fig. 1d). Restriction of the Drake Passage also leads to cooling of the South Atlantic by limiting the amount of relatively temperate Pacific water moving through the Southern Ocean, while Australia warms as it detaches from Antarctica by allowing more ocean flow along its southern margin. Finally, the equatorial Pacific warms with a decline in upwelling and evaporation due to a weaker Pacific Walker circulation (Poulsen et al., 1998).

The lack of a large global TS response to changes in Cretaceous paleogeography in our results is consistent with other recent modeling work (Lunt et al. 2016), but contrasts a previous modeling study on the topic (Donnadieu et al., 2006). The discrepancies between our results and those of Donnadieu et al. (2006) likely come from differences in the climate models. Donnadieu et al. (2006) employ the Fast Ocean Atmosphere Model (Jacob, 1997), which, in contrast with our model configurations, uses lower resolution, a slab ocean, and somewhat different paleogeographies.

Response to Atmospheric ρCO_2

The model responses to a halving of CO_2 are greater than those due to changes in paleogeography (Fig. DR5, DR6c,d). From MAA4x to MAA2x, global mean TS decreases by 3.1 °C and 3.3 °C in CCSM4 and HadCM3L, respectively. Based on our ensemble-mean energy balance calculations, an increase in infrared emissivity is the greatest driver of cooling and causes a 2.45 °C decrease in TS. Albedo feedbacks amplify infrared cooling by 0.75 °C, while an increase in ocean heat transport due to a larger equator-to-pole temperature gradient provides 0.05 °C of warming.

Arctic amplification occurs in both models from MAA4x to MAA2x, but it is also the primary source of discrepancy between simulated TS responses. CCSM4 exhibits larger Arctic sea ice and water vapor feedbacks than HadCM3L (Fig. 1e, DR2, DR5, DR7). In CCSM4, the increase in sea ice cover leads to less evaporation from the ocean, less cloud cover, and less trapped longwave radiation, while reflected shortwave radiation remains high due to high sea-ice albedo (Fig. DR6c,d). Greenland also becomes significantly colder in CCSM4, as vegetation is replaced by bare ground and snow cover increases. These responses are not as pronounced in HadCM3L because Arctic sea ice, vegetation, and cloud cover do not change as significantly. In both models, the greatest SST cooling occurs in the Northern Hemisphere mid-latitudes, possibly due to greater radiative cooling of the nearby large continental area (Fig. 2b-c, DR5b).

The responses in Antarctica between models are also somewhat distinct. Here, drier conditions reduce cloud cover in CCSM4, but this acts to reduce the albedo and dampen polar amplification. Like in the Arctic, HadCM3L cloud-cover decreases relatively less in Antarctica, leading to only small albedo amplification from greater snow-cover. Further, HadCM3L shows warming in the in the Indian and Atlantic sectors of the Southern Ocean due to greater high-latitude deep-water formation, which draws more warm water poleward. Increased salinity resulting from reduced precipitation and runoff around Antarctica appears to drive much of the increased sinking, which is not as pronounced in CCSM4. Overall, the model responses from MAA4x to MAA2x are not spatially uniform, but almost the entire globe experiences some amount of cooling and the first order responses are consistent between models.

DISCUSSION

Proxy Comparison

Our compilation of SST proxies (Table DR2) suggests widespread cooling from the CEN to MAA, with general agreement between different proxy methods in the amount of cooling (Fig. 2a-d). With the current data set, we find no compelling evidence for a significant increase in low-to-mid latitude meridional SST gradients from the CEN to the MAA, as might be anticipated from global cooling. In fact, our SST proxy gradients are slightly steeper in the CEN (0.32 °C per latitude between 0 and 65°) than the MAA (0.29 °C per latitude between 0 and 65°); however, the difference is not statistically significant (see Data Repository). This result agrees with the fish tooth enamel SST reconstructions of Pucéat et al. (2007) and our modeling results (~0.33 °C per latitude between 0 and 65° for all experiments), but disagrees with the PF SST reconstructions of Huber et al. (2002), which suggest a significant reduction in latitudinal SST gradient across Late Cretaceous. The flattening SST gradient in the Huber et al. (2002) reconstructions may be an artifact of diagenesis in some PF records (Pucéat et al., 2007). Not unexpectedly, our proxy-based latitudinal SST gradient increases in both the CEN and MAA if we remove PF reconstructions (Fig. DR8, DR9, DR10), under the justification that they are likely cold biased due to diagenetic alteration (Pearson et al., 2001). Yet, even though the cool tropical SST values from PF suggest post-depositional alteration, the magnitude of PF-based SST cooling from the CEN to MAA is similar to the average SST cooling from the other reconstruction methods in our compilation (between 20°S-20°N, an average cooling of 9.0 °C from PF data versus 7.2 °C for all other proxies data). Regardless of the proxy methods included, latitudinal SST gradients hint at the existence of Arctic sea-ice in the Late Cretaceous, in agreement with both CCSM4 and HadCM3L model results and sea-ice proxy studies (e.g., Bowman et al., 2013).

Amount of Cooling

There are sufficient data to confirm that cooling was widespread and greater than can be explained by a factor of two reduction in atmospheric CO_2 (Fig. 2d, DR5), given model sensitivities of ~3.2 °C. In the low-to-mid latitudes, where sample density is greatest, proxies show an SST cooling of >6 °C while the models suggest a cooling of only 2–4 °C from a halving of CO_2 (Fig. 2d, DR5). Based on our model results, we suspect 1120 ppm CO_2 is too low for the mid-Cretaceous since many SST proxy values are greater than the model simulated values (mean SST difference of +2.27 ± 5.70 (1σ) without PF), particularly in the tropical region (Fig. DR11). Greater than 1120 ppm CO_2 values during the CEN are within proxy reconstruction uncertainty (Wang et al., 2014) as is potential warming from other GHGs such as methane (Beerling and Royer, 2011). In contrast, the MAA2x simulations match SST proxies fairly well and only show a small warm bias (mean SST difference of −0.65 ± 4.16 (1σ) without PF).

Limitations

Data scarcity limits the extent of our comparisons. High-latitude SST changes remain uncertain due to a lack of available proxy data, making validation of our model simulated responses difficult. Further, the available SST proxies are too few and spatially biased to calculate representative global average SSTs for either the CEN or MAA.

Specifically, the CEN records are located mostly in the Tethys and Atlantic, with few data in the Pacific, while the MAA records are located mostly in the Atlantic. For both stages, records come mainly from the Northern Hemisphere (Fig. DR1). Further, the CEN records that have high-resolution ages, especially those from mid-latitude regions, are skewed toward the lower CEN, which might bias the compilation to particular variability within the stage; in contrast, the MAA data are fairly well distributed over the stage.

Proxy uncertainties are also problematic. In this study, we chose to explore only the marine realm because ocean temperatures have a smaller interannual range, and therefore, are more likely to be representative of mean climate conditions. Still, seasonal bias and diagenetic effects likely affect our results. We avoid comparing our model results with LST proxies due to difficulties such as the substantial heterogeneity over small spatial scales due to topography that cannot be resolved by the models and greater seasonality that might bias temperatures (e.g., Spicer et al., 2008; Upchurch et al., 2015).

CONCLUSIONS

The compilation of SST proxies shows that the Late Cretaceous cooling was widespread. Our model results confirm that a reduction in GHG concentrations, not paleogeographic evolution, can explain the majority of the global cooling. Previous proxy temperature comparisons (Pucéat et al., 2007; Linnert et al., 2014), and CO_2 reconstructions (e.g., Wang et al., 2014) support our findings. Nevertheless, paleogeographic changes do cause substantial region climate responses that are important for interpreting regional climate variability in proxy records.

While SSTs agree to first order between models and proxies, significant LST discrepancies remain, particularly in Central Siberia (e.g., Spicer et al., 2008). The continuing model/proxy disagreement in the Siberian interior might represent missing model features such as heterogeneous topography (Spicer et al., 2008), small-scale waterways (Upchurch et al., 2015), vegetation differences (e.g., Otto-Bliesner and Upchurch, 1997), chemistry/climate interactions (e.g., Kump and Pollard, 2008), or a reduction in O_2 levels (Poulsen et al., 2015). However, a lack of direct evidence for these alternative warming mechanisms makes their potential impacts difficult to assess.

ACKNOWLEDGMENTS

We thank Tracy Frank and two anonymous reviewers for their thoughtful comments that greatly improved this manuscript. We also appreciate the efforts of editor Judith Parrish and the helpful discussion with Rich Fiorella. For the CCSM4 experiments, we acknowledge high-performance computing support from the Yellowstone supercomputer provided by NCAR's Computational and Information Systems Laboratory, sponsored by the National Science Foundation. We thank Getech Plc for their paleogeography reconstructions. This work was supported by NSF OCE grant 1261443 to C.J. Poulsen. The HadCM3L simulations were carried out in the framework of NERC grants NE/I005722/1 and NE/K014757/1.

REFERENCES CITED

Beerling, D.J., and Royer, D.L., 2011, Convergent Cenozoic CO_2 history: Nature Geoscience, v. 4, p. 418–420, doi:10.1038/ngeo1186.

Bowman, V.C., Francis, J.E., and Riding, J.B., 2013, Late Cretaceous winter sea ice in Antarctica?: Geology, v. 41, p. 1227–1230, doi:10.1130/G34891.1.

Boyce, C.K., Brodribb, T.J., Feild, T.S., and Zwieniecki, M.A., 2009, Angiosperm leaf vein evolution was physiologically and environmentally transformative:

Proceedings. Biological Sciences, v. 276, p. 1771–1776, doi:10.1098/rspb.2008.1919.

Broecker, W.S., 1989, The Salinity Contrast Between the Atlantic and Pacific Oceans During Glacial Time: Paleoceanography, v. 4, p. 207–212, doi:10.1029/PA004i002p00207.

Donnadieu, Y., Pierrehumbert, R., Jacob, R., and Fluteau, F., 2006, Modelling the primary control of paleogeography on Cretaceous climate: Earth and Planetary Science Letters, v. 248, p. 426–437, doi:10.1016/j.epsl.2006.06.007.

Friedrich, O., Norris, R.D., and Erbacher, J., 2012, Evolution of middle to Late Cretaceous oceans—A 55 m.y. record of Earth’s temperature and carbon cycle: Geology, v. 40, p. 107–110, doi:10.1130/G32701.1.

Gough, D.O., 1981, Solar interior structure and luminosity variations: Physics of Solar Variations, v. 74, p. 21–34, doi:10.1007/BF00151270.

Huber, B.T., Norris, R.D., and MacLeod, K.G., 2002, Deep-sea paleotemperature record of extreme warmth during the Cretaceous: Geology, v. 33, p. 437–440.

Jacob, R., 1997, Low frequency variability in a simulated atmosphere ocean system [Ph.D. Thesis]: Madison, University of Wisconsin, 159 p.

Kump, L.R., and Pollard, D., 2008, Amplification of Cretaceous Warmth by Biological Cloud Feedbacks: Science, v. 320, p. 195–195, doi:10.1126/science.1153883.

Linnert, C., Robinson, S.A., Lees, J.A., Bown, P.R., Pérez-Rodríguez, I., Petrizzo, M.R., Falzoni, F., Littler, K., Arz, J.E.A., and Russell, E.E., 2014, Evidence for global cooling in the Late Cretaceous: Nature Communications, v. 5, p. 1–7, doi:10.1038/ncomms5194.

Lunt, D.J., Farnsworth, A., Loptson, C., Foster, G.L., Markwick, P., O'Brien, C.L., Pancost, R.D., Robinson, S.A., and Wrobel, N., 2016, Palaeogeographic controls on climate and proxy interpretation: Climate of the Past, v. 11, p. 5683–5725, doi:10.5194/cpd-11-5683-2015.

Markwick, P.J., and Valdes, P.J., 2004, Palaeo-digital elevation models for use as boundary conditions in coupled ocean–atmosphere GCM experiments: A Maastrichtian (late Cretaceous) example: Palaeogeography, Palaeoclimatology, Palaeoecology, v. 213, p. 37–63, doi:10.1016/S0031-0182(04)00330-X.

Otto-Bliesner, B.L., and Upchurch, G.R., Jr., 1997, Vegetation-induced warming of high-latitude regions during the Late Cretaceous period: Nature, v. 385, p. 804–807, doi:10.1038/385804a0.

Pearson, P.N., Ditchfield, P.W., Singano, J., Harcourt-Brown, K.G., Nicholas, C.J., Olsson, R.K., Shackleton, N.J., and Hall, M.A., 2001, Warm tropical sea TSs in the Late Cretaceous and Eocene epochs: Nature, v. 413, p. 481–487, doi:10.1038/35097000.

Poulsen, C.J., Barron, E.J., Peterson, W.H., and Wilson, P.A., 1999, A reinterpretation of mid-Cretaceous shallow marine temperatures through model-data comparison: Paleoceanography, v. 14, p. 679–697, doi:10.1029/1999PA900034.

Poulsen, C.J., Seidov, D., Barron, E.J., and Peterson, W.H., 1998, The impact of paleogeographic evolution on the surface oceanic circulation and the marine environment within the mid-Cretaceous Tethys: Paleoceanography, v. 13, p. 546–559, doi:10.1029/98PA01789.

Poulsen, C.J., Tabor, C., and White, J.D., 2015, Long-term climate forcing by atmospheric oxygen concentrations: Science, v. 348, p. 1238–1241, doi:10.1126/science.1260670.

Pucéat, E., Lécuyer, C., Donnadieu, Y., Naveau, P., Cappetta, H., Ramstein, G., Huber, B.T., and Kriwet, J., 2007, Fish tooth δ18O revising Late Cretaceous meridional upper ocean water temperature gradients: Geology, v. 35, p. 107, doi:10.1130/G23103A.1.

Rosenbloom, N.A., Otto-Bliesner, B.L., Brady, E.C., and Lawrence, P.J., 2013, Simulating the mid-Pliocene Warm Period with the CCSM4 model: Geoscientific Model Development, v. 6, p. 549–561, doi:10.5194/gmd-6-549-2013.

Sewall, J.O., van de Wal, R.S.W., van der Zwan, K., van Oosterhout, C., Dijkstra, H.A., and Scotese, C.R., 2007, Climate model boundary conditions for four Cretaceous time slabs: Climate of the Past, v. 3, p. 647–657, doi:10.5194/cp-3-647-2007.

Shackleton, N.J., and Kennett, J.P., 1975, Paleotemperature history of the Cenozoic and the initiation of Antarctic glaciation: Oxygen and carbon isotope analyses in DSDP sites 277, 279, and 281: DSDP, v. 729, doi:10.2973/dsdp.proc.29.117.1975.

Spicer, R.A., Ahlberg, A., Herman, A.B., Hofmann, C.C., Raikevich, M., Valdes, P.J., and Markwick, P.J., 2008, The Late Cretaceous continental interior of Siberia: A challenge for climate models: Earth and Planetary Science Letters, v. 267, p. 228–235, doi:10.1016/j.epsl.2007.11.049.

Upchurch, G.R., Jr., Kiehl, J., Shields, C., Scherer, J., and Scotese, C., 2015, Latitudinal temperature gradients and high-latitude temperatures during the latest Cretaceous:

Congruence of geologic data and climate models: Geology, v. 43, p. 683–686, doi:10.1130/G36802.1.

Wang, Y., Huang, C., Sun, B., Quan, C., Wu, J., and Lin, Z., 2014, Paleo-CO_2 variation trends and the Cretaceous greenhouse climate: Earth-Science Reviews, v. 129, p. 136–147, doi:10.1016/j.earscirev.2013.11.001.

FIGURE CAPTIONS

Figure 1. Late Cretaceous mean annual TS and differences. Column 1 shows the ensemble-average mean-annual TS of CCSM4 and HadCM3L from CEN4x (A), MAA4x (B), and MAA2x (C). Column 2 shows the difference in ensemble-average mean-annual TS of CCSM4 and HadCM3L between CEN4x and MAA4x (D), MAA4x and MAA2x (E), and CEN4x and MAA2x (F). Column 3 shows the mean-annual TS differences between CCSM4 and HadCM3L for CEN4x (G), MAA4x (H), and MAA2x (I).

Figure 2. Proxy data and model zonal mean SSTs for A) CEN4x, B) MAA4x, and C) MAA2x. D) All proxy data and Gaussian fits colored by age. In this figure: model SSTs are from 5-m depth, the blue lines represent the multi-model zonal mean SST gradients and the blue shadings represents the simulated range of zonal mean SSTs from HadCM3L and CCSM4; vertical lines over proxy data represent uncertainty; black dots are model SST values at proxy locations and overlaid vertical lines are the multi-model bounds of HadCM3L and CCSM4; maroon lines show Gaussian best fits of the proxy data between 65°S/N. Gaussian fits of the proxies in panels A), B), and C) include an

adjustment for the deviation of the SSTs from the zonal mean based on model-simulated longitudinal heterogeneity in order to create a more representative proxy latitudinal gradient (see Data Repository). In panel D), blue and red shading show 90% confidence intervals of the Gaussian best fits. Shells designate all non-foraminifera shells including mollusks, bivalves, brachiopods, and belemnite rosta.

[1] GSA Data Repository item 201Xxxx, additional methods, supplemental Figures DR1-11, Table DR1,2, and data sources, is available online at www.geosociety.org/pubs/ft20XX.htm, or on request from editing@geosociety.org.

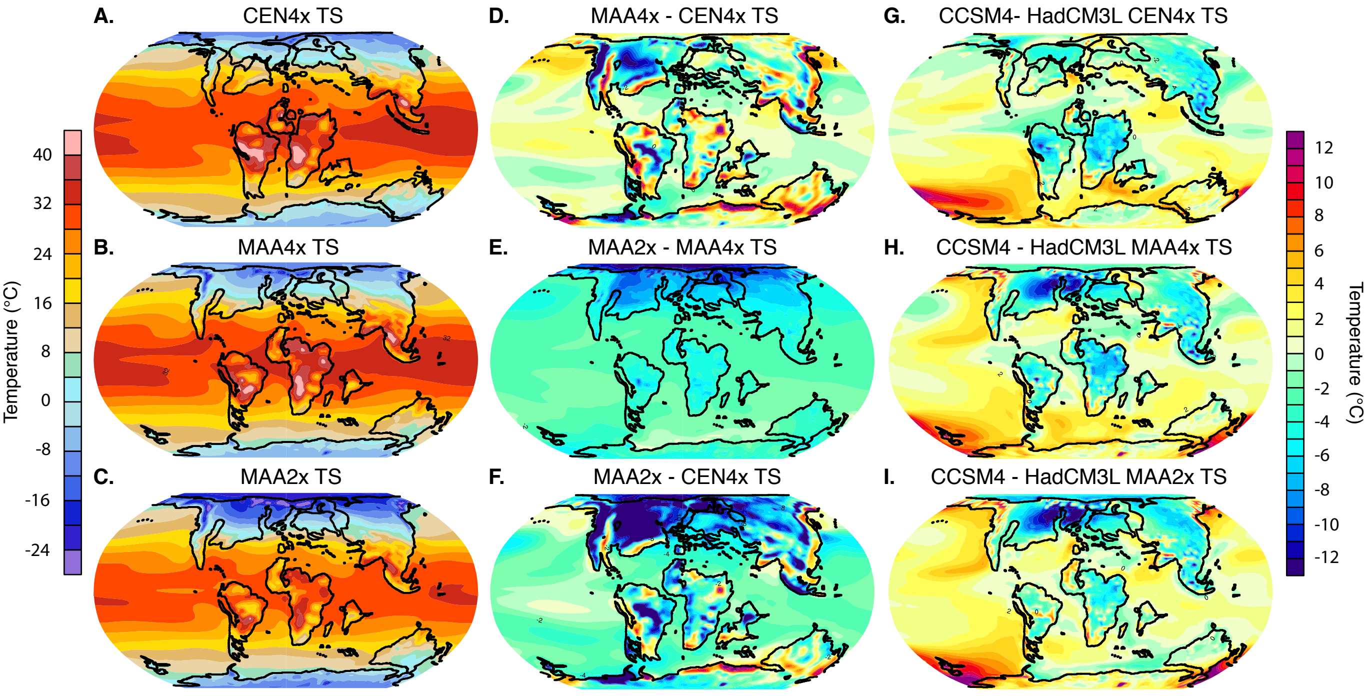

A. CEN4x TS
B. MAA4x TS
C. MAA2x TS
D. MAA4x - CEN4x TS
E. MAA2x - MAA4x TS
F. MAA2x - CEN4x TS
G. CCSM4- HadCM3L CEN4x TS
H. CCSM4 - HadCM3L MAA4x TS
I. CCSM4 - HadCM3L MAA2x TS
Temperature (°C)
40
32
24
16
8
0
-8
-16
-24
Temperature (°C)
12
10
8
6
4
2
0
-2
-4
-6
-8
-10
-12

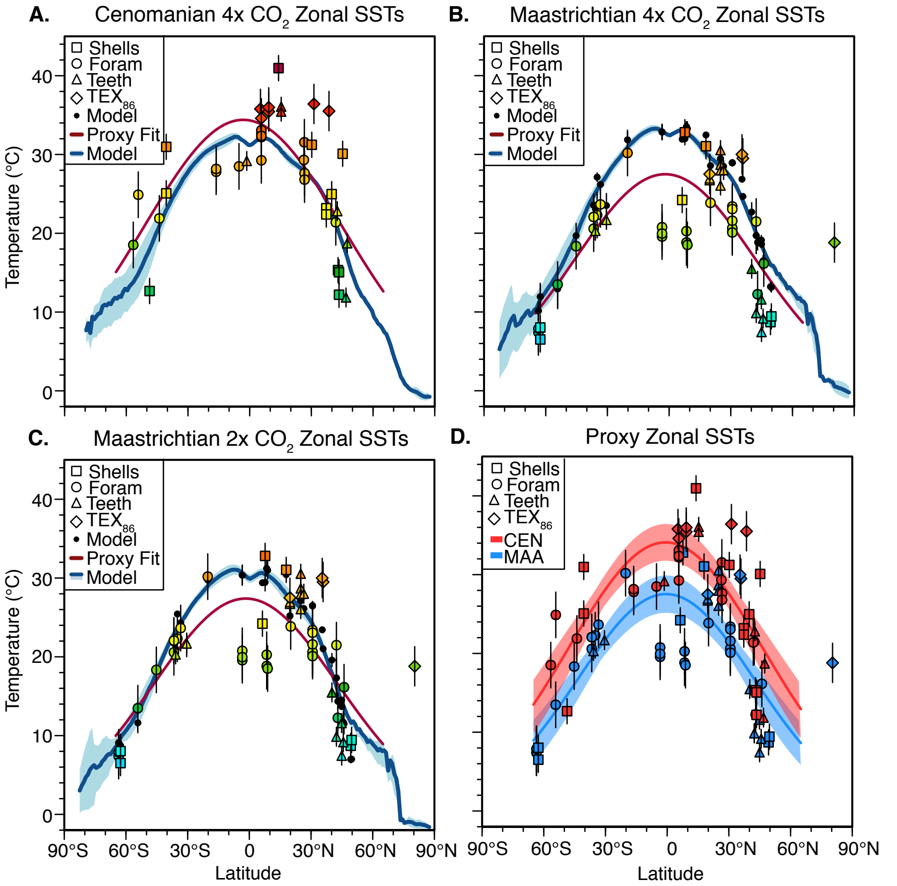
A.
Cenomanian 4x CO_2 Zonal SSTs
B.
Maastrichtian 4x CO_2 Zonal SSTs
C.
Maastrichtian 2x CO_2 Zonal SSTs
D.
Proxy Zonal SSTs
Shells
Foram
Teeth
TEX_{86}
Model
Proxy Fit
Model
CEN
MAA
Temperature (°C)
Latitude
0
10
20
30
40
90°S
60°S
30°S
0
30°N
60°N
90°N

The cause of Late Cretaceous cooling: a multi-model/proxy comparison

Clay R. Tabor[1,2], Christopher J. Poulsen[1], Daniel J. Lunt[3], Nan A. Rosenbloom[2], Bette L. Otto-Bliesner[2], Paul J. Markwick[4], Esther C. Brady[2], Alexander Farnsworth[3], and Ran Feng[2]

[1] *Department of Earth and Environmental Sciences, University of Michigan, 2534 C. C. Little Building, 1100 North University Ave, Ann Arbor, MI 48109*

[2] *National Center for Atmospheric Research, 1850 Table Mesa Dr, Boulder, CO 80305*

[3] *School of Geographic Sciences, University of Bristol, University Road, Clifton, Bristol BS8 1SS*

[4] *Getech, Kitson House, Elmete Hall, Elmete Lane, Leeds, LS8 2LJ*

GSA DATA REPOSITORY

MODEL DESCRIPTIONS

CCSM4

We use the Community Climate System Model version 4 (CCSM4) maintained at the National Center for Atmospheric Research (NCAR). Our model component-set includes the Community Atmospheric Model version 4 (CAM4), the Community Land Model version 4 with dynamic vegetation (CLM4-DGVM), the Parallel Ocean Project model version 2 (POP2), and the Community Sea Ice model version 4 (CICE4). Additional details on the model components and performance can be found in Gent et al. (2011), and information on the DGVM is documented in Levis et al. (2004). The ocean and sea ice models run on a rotated poles grid at roughly 1° resolution with 60 vertical ocean levels. The atmosphere and land-surface models run on a finite-volume grid of 1.9×2.5°, and the atmosphere has 28 vertical levels. We run CAM4 with the Bulk Aerosol Model (BAM), a prognostic aerosol model, with aerosol concentrations and types adjusted for the Cretaceous using a method similar to Heavens et al. (2012). Here, aerosol data come from pre-industrial datasets converted into hemispherically symmetric, monthly zonal average aerosols distributions masked independently to land and sea. In addition, we add the land black carbon emissions from 62.5°N/S to all latitudes further poleward to reflect the greater vegetation cover and fire potential at high latitudes during the Cretaceous (Upchurch et al., 1998). We run all simulations for 1500 years with all model components active and synchronously coupled.

HadCM3L

We also use the Hadley Centre Model (HadCM), developed by the UK Met Office. For this study, we implement HadCM3L version 4.5, which contains dynamic atmosphere, ocean, land, and sea ice components on a 2.5x3.75° grid. The ocean and atmosphere have 19 and 20 vertical levels, respectively. Description of the similar HadCM3 model is documented in Gordon et al. (Gordon et al., 2000). We couple HadCM3L with the Top-down Representation of Interactive Foliage and Flora Including Dynamics (TRIFFID) model with the land surface scheme MOSES 2.1 to simulate dynamic vegetation (Cox, 2001). We run the HadCM3 experiments in 4 phases:

1. 50 years with 280 ppm CO_2 and bare-ground
2. 319 years of either 560 or 1120 ppm CO_2 with TRIFFID turned on

3. 53 years with the addition of prescribed lakes
4. 1000 years with barotropic ocean flow enabled to allow non-zero vertically integrated ocean flow

For additional details on HadCM3L initialization and spin-up see Lunt et al. (2015).

MODELS SETUP

Simulations use the paleogeographic reconstructions of Getech Plc. Following model standard practices and for improved stability, we apply model specific smoothing to the topography. For both models, we adjust total TSI for the Cenomanian (CEN) and Maastrichtian (MAA) based on the equation of Gough (1981). We prescribe CO_2 concentrations as either 4x (1120 ppm) or 2x preindustrial (560 ppm). All other GHG concentrations are set to preindustrial values of 790 ppb for CH_4, 275 ppb for N_2O, and no CFCs. The orbit configuration is set to present-day. Vegetation plant functional types are model defaults; we make no adjustments for the Cretaceous. All simulations run long enough for the upper ocean to reach near-equilibrium; however, the deep ocean continues to adjust. As a result, we focus only on surface conditions.

ENERGY BALANCE CALCULATIONS

We use the zonal mean energy balance decomposition method of Heinemann (2009), which was subsequently adopted and modified by Lunt et al. (2012), and Hill et al. (2014), to explore the mechanisms responsible for surface temperature change in the Late Cretaceous with changes in paleogeography and CO_2. This method assumes incoming shortwave balances with outgoing longwave and that local imbalances are due to changes heat convergence, using the following relationship:

$$\frac{S_0}{4}(1-\alpha)+H=\varepsilon\sigma T^4 \ . (1)$$

Here, S_0 is TSI, α is albedo, H is meridional heat convergence, ε is emissivitiy, σ (5.67×10^{-8} $Wm^{-2}K^{-4}$) is the Stefan-Boltzmann constant, and T is surface temperature. With the exception of σ, values in equation (1) come from zonal averages of Earth system model outputs. We can rewrite equation (1) with respect to surface temperature as:

$$T=(\frac{1}{\varepsilon\sigma}\left(\frac{S_0}{4}(1-\alpha)+H\right)^{0.25})\equiv E(\varepsilon,\alpha,H) \ . (2)$$

By substituting variables from different simulations and differencing them, we can deconstruct the various contributions to the change in surface temperature. We illustrate this below:

$$\Delta T_{emm}=E(\varepsilon,\alpha,H)-E(\varepsilon',\alpha,H) \ . (3)$$

$$\Delta T_{alb}=E(\varepsilon,\alpha,H)-E(\varepsilon,\alpha',H) \ . (4)$$

$$\Delta T_{tran}=E(\varepsilon,\alpha,H)-E(\varepsilon,\alpha,H') \ . (5)$$

where ΔT_{emm}, ΔT_{alb}, and ΔT_{tran} are contributions from emissivity, albedo, and heat convergence to surface temperature change, and primes represent the zonal averages from the simulations being compared. The combination of surface temperature changes due to emissivity, albedo, and heat convergence sum to approximate the total surface temperature response:

$$\Delta T_{total}\cong\Delta T_{emm}+\Delta T_{alb}+\Delta T_{tran} \ . (6)$$

This technique can be used to further decompose the climate contributions to surface temperature.

PROXY DATA

As mentioned in the main text, SST proxy values represent location and age averages.

Method uncertainties only accounts for calibration uncertainties. We apply these uncertainties to every averaged data point. The range in values from a particular age and site are often significantly greater than the calibration uncertainties. Therefore, uncertainties represent minimum estimates.

Point locations are consistently rotated back in time from their present-day sampling locations to the CEN and MAA using the plate reconstructions from Getech Plc. Occasionally, the coarse model resolutions result in marine proxy paleo-locations over land instead of water. In these situations, we select the nearest model ocean location to represent the SST value.

To create more representative latitudinal SST gradients, Gaussian fits of the proxies include an adjustment for the deviation of the SSTs from the zonal mean based on model-simulated longitudinal heterogeneity. For example, if an equatorial proxy location has a model simulated SST of 30°C and a model zonal mean equatorial SST of 35°C, then 5°C are added to the proxy value so that it is in better agreement with the zonal average. This technique assumes that model longitudinal variability is robust regardless of mean SSTs.

We investigate the statistical similarity between the temperature gradients of our CEN and MAA datasets using an F-test. An F-test determines if the variance of multiple datasets are statistically different from each other. To standardize the data, we first remove the global means of the Gaussian fitting procedure (Fig. 2d). Then, we apply an F-test to test the hypothesis that the spread of residual SSTs between the CEN and MAA are statistically distinct. Our results produce a p-value equal to 0.386, which suggests that SST variations, except for the means between datasets, are not robust.

Seawater $\delta^{18}O$

We assume a mean $\delta^{18}O_{sw}$ of $-1^{0}/_{00}$ VSMOW, based on the assumption of an ice-free world (Shackleton and Kennett, 1975). This assumption is widely used in Cretaceous SST reconstructions (e.g. Huber et al., 2002; Friedrich et al., 2012); however, debate remains about the potential for glaciation in the Late Cretaceous (e.g. Miller et al., 2005). A significant increase in land-ice would require less cooling in the MAA from $\delta^{18}O$ records but is not considered further in this study.

$\delta^{18}O_{sw}$ has significant regional variability in both the modern and Late Cretaceous (Zhou et al., 2008). To account for this variability, we use zonal average salinity from the model outputs with the present-day salinity/$\delta^{18}O_{sw}$ relationship of Broecker (1989). This simple linear relationship follows:

$$\delta^{18}O_w = 0.5(PSU) - 17.12 \ . \quad (7)$$

where PSU stands for positive salinity units. In our simulations, mean ocean salinity starts at 35 PSU, which is equivalent to present-day. While not perfect, we prefer this relationship to the commonly employed present-day latitudinal $\delta^{18}O_{sw}$ correction by Zachos et al. (1994), because it indirectly accounts for precipitation and evaporation, and does not make present-day assumptions about the latitudinal distribution of $\delta^{18}O_{sw}$ (Poulsen et al., 1999). Still, this technique is inferior to model experiments that include water isotope tracking (e.g. Zhou et al., 2008).

Planktonic Foraminifera

We calculate SSTs from $\delta^{18}O$ measurements of planktonic foraminifera using the calibration of Erez and Luz (1983) and a conversion to VSMOW of $0.22^{0}/_{00}$ (Bemis et al., 1998). This calibration has been widely used for foraminifera temperature reconstructions and proven accurate for a wide range of temperatures. Temperatures are calculated using the polynomial:

$$T(°C) = 16.998 - 4.52[\delta^{18}O_c - (\delta^{18}O_{sw} + 0.22)] + 0.028[\delta^{18}O_c - (\delta^{18}O_{sw} + 0.22)]^2 \ . \ (8)$$

where $\delta^{18}O_c$ is the $\delta^{18}O$ of sample calcite.

Diagenetic alteration is a potential issue for foraminifera, causing them to pickup post-depositional temperature signals from the ocean floor (e.g. Pearson et al., 2001; Norris et al., 2002). It is likely that some of the foraminifera presented in this study suffer from such alteration given the sample descriptions, relatively cool tropical SSTs, and disagreement with other SST proxy values. However, given the paucity of records and uncertainty in other included proxy techniques such as TEX_{86} (e.g. Taylor et al., 2013), we opt to include all planktonic foraminifera data. For comparison, we include zonal SST reconstructions without foraminifera as well (Fig. DR8, DR9, DR10). Even though removal of foraminifera leads to warmer tropical SST reconstructions, it does not significantly change the magnitude of cooling from the CEN to the Maa, which is the main focus of this study. We assign an uncertainty of $\pm$2.9°C for planktonic foraminifera based on Holocene core-top data from Crowley and Zachos (Crowley and Zachos, 2000) and to be consistent with the work of Upchurch (2015).

Shells and Others

We use the $\delta^{18}O$ to temperature conversion of Anderson and Arthur (1983) for both aragonite and calcite of shells of mollusks, bivalves, brachiopods, and belemnite rosta based on its prevalent use in the proxy source literature. The equation is:

$$T(°C) = 16.4 - 4.14(\delta^{18}O_{c/a} - \delta^{18}O_{sw}) + 0.13(\delta^{18}O_{c/a} - \delta^{18}O_{sw})^2 \;. (9)$$

where $\delta^{18}O_{c/a}$ is the $\delta^{18}O$ of sample calcite or aragonite. Like foraminifera, shells are prone to alteration (Steuber et al., 1999). We include all records here for completeness. We also show comparisons with shell SST proxies omitted (Fig. DR8, DR9, DR10). We apply an uncertainty of ±1.6 based on 1σ of a mollusk calibration by Grossman and Ku (1986) as in Upchurch et al. (2015).

Tooth Enamel δ^{18}O

Our SST proxy compilation includes phosphate $\delta^{18}O$ records from fish tooth enamel, most of which were originally compiled by Pucéat et al. (2007). These records are considered more resistant to diagenetic alteration than foraminifera or shells, and were previously used by Pucéat et al. (2007) to argue for a near-modern latitudinal SST gradient in the Cretaceous, in contrast to reconstructions from foraminifera that suggested a shallower latitudinal SST gradient (e.g. Huber et al., 2002). Recently, there have been several recalibrations of the phosphate $\delta^{18}O$ temperature relationship. Here, we use the most recent calibration by Lecuyer et al. (2013):

$$T(°C) = 117.4 - 4.5(\delta^{18}O_{PO4} - \delta^{18}O_{sw}) \;. (10)$$

where $\delta^{18}O_{PO4}$ is the $\delta^{18}O$ of sample phosphate. This calibration results in SSTs that are several degrees warmer than the calibration by Pucéat et al. (2007) and several degrees cooler than the recent calibration by Pucéat et al. (2010). However, the magnitude of offset between calibrations remains quite similar over the range of $\delta^{18}O_{PO4}$ values. Therefore, while the absolute temperature reconstructions differ depending on the chosen calibration, the difference between the CEN and MAA records is small. In addition, the calibration of Lecuyer et al. (2013) benefits from the smallest uncertainty of ±1.2°C, which we apply to all tooth enamel SST values.

TEX_{86}

TEX_{86} is a relatively new SST proxy method based on the ratio of different glycerol dialkyl glycerol tetraethers (GDGTs) with 86 carbons, which comprise membrane lipids in marine Crenarchaeota (Schouten et al., 2002). It has the benefit of not relying on $\delta^{18}O_{sw}$ assumptions. Here, we use the calibration of Kim et al. (2010) TEX_{86}^{H}, which provides the smallest error in warm climate conditions. The equation is:

$$T(°C) = 68.4\log(TEX_{86}) + 38.6\ . \quad (11)$$

Modern calibration by Kim et al. (2010) show an uncertainty of ±2.5°C, which we use in our model/proxy comparison.

We include the high-latitude MAA TEX_{86}^{H} SST value from Jenkyns et al. (2004) in our tables and plots for reference but do not include it in our analyses. We find, like several former studies (Davies et al., 2009; Spicer and Herman, 2010; Upchurch et al., 2015), that this value represents an extreme outlier from other proxy data and model results. Inclusion of this data point significantly skews our results, because it is the only available Arctic MAA SST value. Based on our other findings, it requires roughly 10°C warming from 50°N to 80°N, for which we have no physical basis.

GSA DATA REPOSITORY FIGURE CAPTIONS

Figure DR1. Getech Plc CEN and MAA paleogeography with marine proxy locations.

Figure DR2: Individual model simulated Late Cretaceous mean annual surface temperatures and temperature responses to changes in paleogeography and CO_2 concentration. Row 1 shows

CCSM4 mean annual surface temperatures from CEN4x (A), MAA4x (B), and MAA2x (C). Row 2 shows HadCM3L mean annual surface temperatures from CEN4x (D), MAA4x (E), and MAA2x (F). Row 3 shows CCSM4 mean annual surface temperature differences between CEN4x and MAA4x (G), MAA4x and MAA2x (H), and CEN4x and MAA2x (I). Row 4 shows HadCM3L mean annual surface temperature differences between CEN4x and MAA4x (J), MAA4x and MAA2x (K), and CEN4x and MAA2x (L). The large-scale surface temperature patterns are quite similar for both models.

Figure DR3. Late Cretaceous mean annual total cloud cover and anomalies. Column 1 shows the model total cloud cover from A) CEN4x, B) MAA4x, and C) MAA2x. Column 2 shows the difference in total cloud cover between D) CEN4x and MAA4x, E) MAA4x and MAA2x, and F) CEN4x and MAA2x. Column 3 shows the total cloud cover anomalies between CCSM4 and HadCM3L for G) CEN4x, H) MAA4x, and I) MAA2x. Clouds remain one of the largest uncertainties in climate models. Both models show similar cloud patterns for all model configurations. However, the range of cloud cover between regions is more pronounced in HadCM3L than CCSM4. The configuration of the CCSM4 aerosols for paleoclimate might be partly responsible for the discrepancies in cloud magnitude.

Figure DR4. Late Cretaceous mean annual surface albedo and anomalies. Column 1 shows the model surface albedo from A) CEN4x, B) MAA4x, and C) MAA2x. Column 2 shows the difference in surface albedo between D) CEN4x and MAA4x, E) MAA4x and MAA2x, and F) CEN4x and MAA2x. Column 3 shows the surface albedo anomalies between CCSM4 and HadCM3L for G) CEN4x, H) MAA4x, and I) MAA2x. In the high-latitudes, CCSM4 simulates higher surface albedos than HadCM3L due to differences in sea ice cover and vegetation. CCSM4 tends to produce more sea in the Arctic than HadCM3L, which leads to greater shortwave reflection, especially in the spring and fall. CCSM4 also grows shorter, less dense vegetation than HadCM3L in the polar regions. A lower vegetation and reduced canopy allows for more snow cover of vegetation, which raises the albedo. Tall, dense Antarctic vegetation suggested by paleobotantical reconstructions is not simulated in CCSM4 (e.g. Upchurch et al., 1998). Modification of the vegetation model will be an important step in our future work, as some research shows vegetation can help remedy model/proxy LST discrepancies (e.g. Otto-Bliesner and Upchurch, 1998; Zhou et al., 2012).

Figure DR5. Zonal mean annual SST responses to changing topography and decreasing CO_2 for both CCSM4 and HadCM3L models. Comparison of CCSM4 and HadCM3L outputs highlight the similarities in surface temperature response.

Figure DR6. Decomposition of the simulated changes in zonal mean surface temperature into contributions from heat convergence (red), emissivity (green), albedo (blue), and TSI (yellow) for A) CCSM4 and B) HadCM3L changes in geography, C) CCSM4 and D) HadCM3L changes in CO_2, and E) CCSM4 and F) HadCM3L changes in both geography and CO_2. See Data Repository for details on energy balance calculations.

Figure DR7. Seasonal sea ice exists in all 4x PI CO_2 simulations in agreement with some proxies that find evidence for Arctic sea ice during peak Cretaceous warmth (Davies et al., 2009). The Arctic experiences an increase in sea ice concentration from the CEN to MAA because the Arctic becomes more restricted in the Maa. With a reduction in CO_2, a significant amount of perennial sea ice forms in the Arctic while Antarctic sea ice remains mostly seasonal. This contrast in sea ice between hemispheres is similar to present-day where the restricted Arctic promotes retention of sea ice, and the open ocean Antarctic allows the equator drift and wasting of sea ice.

In all experiments, CCSM4 produces greater Arctic sea ice cover and less Antarctic sea ice cover than HadCM3L. This contrast relates to the differences in open ocean SSTs between models. In general, CCSM4 has greater ocean overturning in the high Southern latitudes, which promotes transports of warm equatorial water poleward and inhibits sea ice formation. In contrast, there is less deep-water formation in the high Northern latitudes in either model. Further, the Late Cretaceous Arctic is quite restricted from the greater ocean, especially in the Maa, which prevents warm open ocean waters from having a large effect.

Figure DR8. Latitudinal temperature gradient reconstructions from the CEN with the systematic removal of SST proxy reconstruction data from individual methods. Simulated CEN4x zonal average SSTs with all CEN proxies SST except A) foraminifera, B) fish tooth enamel, C) shells and related structures, and D) TEX_{86}. Removal of foraminifera leads to a significantly warmer equator and steeper equator-to-pole temperature gradient. This gradient is steeper than model simulated SSTs. It appears likely that some foraminifera are not recording a pure SST signal.

Figure DR9. Latitudinal temperature gradient reconstructions from the MAA with the systematic removal of SST proxy reconstruction data from individual methods. Simulated MAA4x zonal average SSTs with all MAA proxies SST except A) foraminifera, B) fish tooth enamel, C) shells and related structures, and D) TEX_{86}. Like for the Cen, removal of foraminifera leads to a significantly warmer equator and steeper equator-to-pole temperature gradient.

Figure DR10. Identical to figure S7 except with simulated MAA2x data plotted.

Figure DR11. SST model/proxy discrepancies by latitude. A) Differences between CEN proxies and CEN4x simulations. B) Differences between MAA proxies and MAA4x simulations. C) Differences between MAA proxies and MAA2x simulations. In general, the CEN4x simulations have a cold bias while the MAA4x simulations have a warm bias. The MAA2x simulations are in better agreement with SST proxies. A model warm bias remains in the equatorial region in the MAA2x, but this might be a result of diagenetic alteration of planktonic foramina. While beyond the scope of this work, calibration choices also impact model/proxy agreement. For example, the warmer fish tooth enamel calibration of Pucéat et al. (2010) might result in a better agreement between models and proxies for the MAA2x simulations.

GSA DATA REPOSITORY REFERENCES CITED

Abramovich, S., Keller, G., Stüben, D., and Berner, Z., 2003, Characterization of late Campanian and Maastrichtian planktonic foraminiferal depth habitats and vital activities based on stable isotopes: Palaeogeography Palaeoclimatology Palaeoecology, v. 202, no. 1-2, p. 1–29, doi: 10.1016/S0031-0182(03)00572-8.

Alsenz, H., Regnery, J., Ashckenazi-Polivoda, S., Meilijson, A., Ron-Yankovich, L., Illner, P., Abramovich, S., Almogi-Labin, A., Feinstein, S., Berner, Z., and Püttmann, W., 2013, Characterization of late Campanian and Maastrichtian planktonic foraminiferal depth habitats and vital activities based on stable isotopes: Palaeogeography Palaeoclimatology Palaeoecology, v. 392, no. C, p. 350–358, doi: 10.1016/j.palaeo.2013.09.013.

Anderson, T.F., Arthur, M.A., 1983: Stable isotopes of oxygen and carbon and their application to sedimentologic and paleoenvironmental problems: Stable Isotopes in Sedimentary Geology, v. 1, p. 1-151.

Ando, A., Nakano, T., Kaiho, K., and Kobayashi, T., 2009, Onset of seawater 87Sr/86Sr excursion prior to Cenomanian–Turonian Oceanic Anoxic Event 2? New Late Cretaceous strontium isotope curve from the central Pacific Ocean: Journal of Foraminiferal Research, v39, no 4, p. 322-334.

Barrera, E., and Savin, S.M., 1999, Evolution of late Campanian-Maastrichtian marine climates and oceans: Geological Society of American-Special Papers, v. 332.

Bemis, E.B., Spero, H.J., Bijma, J., and Lea, D.W., 1998, Reevaluation of the oxygen isotopic composition of planktonic foraminifera: Experimental results and revised paleotemperature equations: Paleoceanography, v. 13, no. 2, p. 150-160.

Bice, K.L., Birgel, D., Meyers, P.A., Dahl, K.A., Hinrichs, K.U., and Norris, R.D., 2006, A multiple proxy and model study of Cretaceous upper ocean temperatures and atmospheric CO_2 concentrations: Paleoceanography, v. 21, no. 2, doi: 10.1029/2005PA001203.

Broecker, W.S., 1989, The Salinity Contrast Between the Atlantic and Pacific Oceans During Glacial Time: Paleoceanography, v. 4, no. 2, p. 207–212, doi: 10.1029/PA004i002p00207.

Carpenter, S.J., Erickson, J.M., and Holland, F.D., 2003, Migration of a Late Cretaceous fish: Nature, v. 423, no. 6935, p. 70–74, doi: 10.1038/nature01588.

Clarke, L.J., and Jenkyns, H.C., 1999, New oxygen isotope evidence for long-term Cretaceous climatic change in the Southern Hemisphere: Geology, v. 27, no. 8, p. 699–702.

Crowley, T.J., and Zachos, J.C., 2000, Comparison of zonal temperature profiles for past warm time periods: Warm Climates in Earth History, p. 50-76.

Cox, P. M., Betts, R. A., Jones, C. D., Spall, S. A., and Totterdell,I. J.:Modelling vegetation and the carbon cycle as interactive elements of the climate system, in: Meteorology at the Millennium,edited by Pearce, R., pp. 259–279, Academic Press, 2001.

Damste, J.S.S., van Bentum, E.C., Reichart, G.-J., Pross, J., and Schouten, S., 2010, Earth and Planetary Science Letters: Earth and Planetary Science Letters, v. 293, no. 1-2, p. 97–103, doi: 10.1016/j.epsl.2010.02.027.

Davies, A., Kemp, A.E.S., and Pike, J., 2009, Late Cretaceous seasonal ocean variability from the Arctic: Nature, v. 460, no. 7252, p. 254–U118, doi: 10.1038/nature08141.

D'Hondt, S., and Lindinger, M., 1994, A stable isotopic record of the Maastrichtian ocean-climate system: South Atlantic DSDP Site 528: Palaeogeography, v. 112, p. 363-378.

Ditchfield, P.W., Marshall, J.D., and Pirrie, D., 1994, High latitude palaeotemperature variation: New data from the Thithonian to Eocene of James Ross Island, Antarctica: Palaeogeography, v. 107, p. 79-101.

El-Shazly, S., Košťák, M., Kloučková, B., Saber, S.G., Felieh Salama, Y., Mazuch, M., and Žák, K., 2011, Carbon and oxygen stable isotopes of selected Cenomanian and Turonian rudists from Egypt and Czech Republic, and a note on changes in rudist diversity: Bulletin of Geosciences,, p. 209–226, doi: 10.3140/bull.geosci.1151.

Erez, J., and Luz, B., 1983, Experimental paleotemperature equation for planktonic foraminifera:

Geochimica Et Cosmochimica Acta, v. 47, p. 1025-1031.

Frank, T.D., and Arthur, M.A., 1999, Tectonic forcings of Maastrichtian ocean-climate evolution: Paleoceanography, v. 14, no. 2, p. 103–117.

Friedrich, O., Herrle, J.O., Kößler, P., and Hemleben, C., 2004, Early Maastrichtian stable isotopes: changing deep water sources in the North Atlantic?: Palaeogeography Palaeoclimatology Palaeoecology, v. 211, no. 1-2, p. 171–184, doi: 10.1016/j.palaeo.2004.05.004.

Friedrich, O., Erbacher, J., Moriya, K., Wilson, P.A., and Kuhnert, H., 2008, Warm saline intermediate waters in the Cretaceous tropical Atlantic Ocean: Nature Geoscience, v. 1, no. 7, p. 453–457, doi: 10.1038/ngeo217.

Friedrich, O., Herrle, J.O., Wilson, P.A., Cooper, M.J., Erbacher, J., and Hemleben, C., 2009, Early Maastrichtian carbon cycle perturbation and cooling event: Implications from the South Atlantic Ocean: Paleoceanography, v. 24, no. 2, p. n/a–n/a, doi: 10.1029/2008PA001654.

Forster, A., Schouten, S., Baas, M., and Damste, J.S.S., 2007a, Mid-Cretaceous (Albian-Santonian) sea surface temperature record of the tropical Atlantic Ocean: Geology, v. 35, no. 10, p. 919–922, doi: 10.1130/G23874A.1.

Forster, A., Schouten, S., Moriya, K., Wilson, P.A., and Sinninghe Damsté, J.S., 2007b, Tropical warming and intermittent cooling during the Cenomanian/Turonian oceanic anoxic event 2: Sea surface temperature records from the equatorial Atlantic: Paleoceanography, v. 22, no. 1, doi: 10.1029/2006PA001349.

Gent, P.R., Danabasoglu, G., Donner, L.J., Holland, M.M., Hunke, E.C., Jayne, S.R., Lawrence, D.M., Neale, R.B., Rasch, P.J., Vertenstein, M., Worley, P.H., Yang, Z.-L., and Zhang, M., 2011, The Community Climate System Model Version 4: Journal of Climate, v. 24, no. 19, p. 4973–4991, doi: 10.1175/2011JCLI4083.1.

Gordon, C., Cooper, C., Senior, C.A., Banks, H., and Gregory, J.M., 2000, The simulation of SST, sea ice extents and ocean heat transports in a version of the Hadley Centre coupled model without flux adjustments: Climate Dynamics, v. 16, p. 147-168.

Gough, D.O., 1981, Solar interior structure and luminosity variations: Physics of Solar Variations, v. 74, p. 21-34.

Grossman, E.L., and Ku, T.L., 1986, Oxygen and carbon isotope fractionation in biogenic aragonite: temperature effects: Chemical Geology: Isotope Geoscience section, v. 59; p. 59-74.

Gustafsson, M., Holbourn, A., and Kuhnt, W., 2003, Changes in Northeast Atlantic temperature and carbon flux during the Cenomanian/Turonian paleoceanographic event: the Goban Spur stable isotope record: Palaeogeography Palaeoclimatology Palaeoecology, v. 201, no. 1-2, p. 51–66, doi: 10.1016/S0031-0182(03)00509-1.

Heavens, N.G., Shields, C.A., and Mahowald, N.M., 2012, A paleogeographic approach to aerosol prescription in simulations of deep time climate: Journal of Advances in Modeling Earth Systems, v. 4, no. 4, p. n/a–n/a, doi: 10.1029/2012MS000166.

Heinemann, M., Jungclaus, J.H., and Marotzke, J., 2009, Warm Paleocene/Eocene climate as simulated in ECHAM5/MPI-OM: Climate of the Past, v. 5, p. 785-802.

Henderson, R.A., and Price, G.D., 2012, Paleoenvironment and paleoecology from oxygen and carbon isotopes of subtropical mollusks from the Late Cretaceous (Cenomanian) of Bathurst Island, Australia: Palaios, v. 27, no. 9, p. 617–626, doi: 10.2110/palo.2011.p11-120r.

Hill, D.J., Haywood, A.M., Lunt, D.J., Hunter, S.J., Bragg, F.J., Contoux, C., Stepanek, C., Sohl, L., Rosenbloom, N.A., Chan, W.L., Kamae, Y., Zhang, Z., Abe-Ouchi, A., Chandler, M.A., et al., 2014, Evaluating the dominant components of warming in Pliocene climate simulations: Climate of the Past, v. 10, no. 1, p. 79–90, doi: 10.5194/cp-10-79-2014.

Huber, B.T., Hodell, D.A., Hamilton, C.P., 1995, Middle–Late Cretaceous climate of the southern high latitudes: stable isotopic evidence for minimal equator-to-pole thermal gradients: Geological Society of America, v. 107, no. 10, p. 1164-1191.

Jenkyns, H.C., Forster, A., Schouten, S., and Damste, J., 2004, High temperatures in the Late Cretaceous Arctic Ocean: Nature, v. 432, no. 7019, p. 888–892, doi: 10.1038/nature03143.

Kim, J.H., van der Meer, J., Schouten, S., Helmke, P., Willmott, V., Sangiorgi, F., Koç, N., Hopmans, E.C., and Damste, J.S.S., 2010, New indices and calibrations derived from the distribution of crenarchaeal isoprenoid tetraether lipids: Implicationsfor past sea surface temperature reconstructions: Geochimica Et Cosmochimica Acta, v. 74, no. 16, p. 4639–4654, doi: 10.1016/j.gca.2010.05.027.

Kolodny, Y., and Raab, M., 1988, Oxygen isotopes in phosphatic fish remains from Israel: paleothermometry of tropical Cretaceous and Tertiary shelf waters: Palaeogeography, v.

64, p. 59-67.

Kolodny, Y., and Luz, B., 1991, Oxygen isotopes in phosphates of fossil fish—Devonian to Recent: The Geochemical Society, p. 105-119.

Lécuyer, C., Amiot, R., Touzeau, A., and Trotter, J., 2013, Calibration of the phosphate d18O thermometer with carbonate-water oxygen isotope fractionation equations: Chemical Geology, v. 347, no. C, p. 217–226, doi: 10.1016/j.chemgeo.2013.03.008.

Lécuyer, C., Grandjean, P., O'Neil, J.R., and Cappetta, H., 1993, Thermal excursions in the ocean at the Cretaceous—Tertiary boundary (northern Morocco): δ 18 O record of phosphatic fish debris: Palaeogeography, v. 105, p. 235-243.

Levis, S., Bonan, G.B., Vertenstein, M., and Oleson, K.W., 2004, The Community Land Model's Dynamic Global Vegetation Model (CLM-DGVM): Technical Description and User"s Guide: National Center For Atmospheric Research.

Li, L.Q., and Keller, G., 1998, Maastrichtian climate, productivity and faunal turnovers in planktic foraminifera in south Atlantic DSDP sites 525A and 21: Marine Micropaleontology, v. 33, no. 1-2, p. 55–86.

Li, L., and Keller, G., 1999, Variability in Late Cretaceous climate and deep waters: evidence from stable isotopes: Marine Geology, v. 161, p. 171-190.

Linnert, C., Robinson, S.A., Lees, J.A., Bown, P.R., guez, I.P.E.R.-R.I., Petrizzo, M.R., Falzoni, F., Littler, K., Arz, J.E.A., and Russell, E.E., 2014, Evidence for global cooling in the Late Cretaceous: Nature Communications, v. 5, p. 1–7, doi: 10.1038/ncomms5194.

Lunt, D.J., Dunkley Jones, T., Heinemann, M., Huber, M., LeGrande, A., Winguth, A., Loptson, C., Marotzke, J., Roberts, C.D., Tindall, J., Valdes, P., and Winguth, C., 2012, A model–data comparison for a multi-model ensemble of early Eocene atmosphere–ocean simulations: EoMIP: Climate of the Past, v. 8, no. 5, p. 1717–1736, doi: 10.5194/cp-8-1717-2012-supplement.

Lunt, D. J., Farnsworth, A., Loptson, C., Foster, G. L., Markwick, P., O'Brien, C. L., Pancost, R. D., Robinson, S. A., and Wrobel, N., 2016, Palaeogeographic controls on climate and proxy interpretation, Clim. Past., 11, 5683-5725, doi:10.5194/cp-12-1181-2016.

Macleod, K.G., Huber, B.T., and Isaza-Londoño, C., 2005, North Atlantic warming during global cooling at the end of the Cretaceous: Geology, v. 33, no. 6, p. 437, doi: 10.1130/G21466.1.

Maestas, Y., MacLeod, K.G., Douglas, R., Self-Trail, J., and Ward, P.D., 2003, Late Cretaceous foraminifera, paleoenvironments, and paleoceanography of the Rosario Formation, San Antonio del Mar, Baja California, Mexico: Journal of Foraminiferal Research, v. 33, no. 3, p. 179–191.

Miller, K.G., et al. 2005, The Phanerozoic Record of Global Sea-Level Change: Science, v. 310, no. 5752, p. 1293–1298, doi: 10.1126/science.1116412.

Moriya, K., Wilson, P.A., Friedrich, O., Erbacher, J., and Kawahata, H., 2007, Testing for ice sheets during the mid-Cretaceous greenhouse using glassy foraminiferal calcite from the mid-Cenomanian tropics on Demerara Rise: Geology, v. 35, no. 7, p. 615–618, doi: 10.1130/G23589A.1.

Norris, R.D., and Wilson, P.A., 1998, Low-latitude sea-surface temperatures for the mid-

Cretaceous and the evolution of planktic foraminifera: Geology, v. 26, no. 9, p. 832-826.
Norris, R.D., Bice, K.L., Magno, E.A., and Wilson, P.A., 2002, Jiggling the tropical thermostat in the Cretaceous hothouse: Geology, v. 30, no. 4, p. 299-302.
Ounis, A., Kocsis, L., Chaabani, F., and Pfeifer, H.-R., 2008, Rare earth elements and stable isotope geochemistry (δ13C and δ18O) of phosphorite deposits in the Gafsa Basin, Tunisia: Palaeogeography Palaeoclimatology Palaeoecology, v. 268, no. 1-2, p. 1–18, doi: 10.1016/j.palaeo.2008.07.005.
Pearson, P.N., Ditchfield, P.W., Singano, J., Harcourt-Brown, K.G., Nicholas, C.J., Olsson, R.K., Shackleton, N.J., and Hall, M.A., 2001, Warm tropical sea surface temperatures in the Late Cretaceous and Eocene epochs: Nature, v. 413, no. 6855, p. 481–487.
Pirrie, D., and Marshall, J.D., 1990, High-paleolatitude late Cretaceous paleotemperatures: new data from James Ross Island, Antarctica: Geology, v. 18, p. 31-34.
Poulsen, C.J., Barron, E.J, Peterson, W.H., and Wilson, P.A.,1999, A reinterpretation of mid-Cretaceous shallow marine temperatures through model-data comparison: Paleoceanography, v. 14, p. 679-697.
Price, G.D., Sellwood, B.W., and Corfield, R.M., 1998, Isotopic evidence for palaeotemperatures and depth stratification of Middle Cretaceous planktonic foraminifera from the Pacific Ocean: Geological Magazine, v. 135, no. 2, p. 183-191.
Price, G.D., and Hart, M.B., 2002, Isotopic evidence for Early to mid-Cretaceous ocean temperature variability: Marine Micropaleontology, v. 46, p. 45-48.
Price, G.D., Williamson, T., Henderson, R.A., and Gagan, M.K., 2012, Barremian-Cenomanian

palaeotemperatures for Australian seas based on new oxygen-isotope data from belemnite rostra: Palaeogeography Palaeoclimatology Palaeoecology, v. 358-360, no. C, p. 27–39, doi: 10.1016/j.palaeo.2012.07.015.

Pucéat, E., Joachimski, M.M., Bouilloux, A., Monna, F., Bonin, A., Motreuil, S., Morinière, P., Hénard, S., Mourin, J., Dera, G., and Quesne, D., 2010, Earth and Planetary Science Letters: Earth and Planetary Science Letters, v. 298, no. 1-2, p. 135–142, doi: 10.1016/j.epsl.2010.07.034.

Pucéat, E., Lécuyer, C., Sheppard, S.M.F., Dromart, G., Reboulet, S., and Grandjean, P., 2003, Thermal evolution of Cretaceous Tethyan marine waters inferred from oxygen isotope composition of fish tooth enamels: Paleoceanography, v. 18, no. 2, p. n/a–n/a, doi: 10.1029/2002PA000823.

Pucéat, E., Lécuyer, C., Donnadieu, Y., Naveau, P., Cappetta, H., Ramstein, G., Huber, B.T., and Kriwet, J., 2007, Fish tooth δ18O revising Late Cretaceous meridional upper ocean water temperature gradients: Geology, v. 35, no. 2, p. 107, doi: 10.1130/G23103A.1.

Schönfeld, J., Sirocko, F., and Jørgensen, N.O., 1991, Oxygen isotope composition of Upper Cretaceous chalk at Lägerdorf (NW Germany): its original environmental signal and palaeotemperature interpretation: Cretaceous Research, v.12, p. 27-46.

Sellwood, B.W., Price, G.D., and Valdest, P.J., 1994, Cooler estimates of Cretaceous temperatures: Nature, v. 370, p. 453-455.

Schouten, S., Hopmans, E.C., Schefuss, E., and Damste, J., 2002, Distributional variations in marine crenarchaeotal membrane lipids: a new tool for reconstructing ancient sea water temperatures?: Earth and Planetary Science Letters, v. 204, no. 1-2, p. 265–274.

Schouten, S., Hopmans, E.C., Forster, A., van Breugel, Y., Kuypers, M.M.M., and Sinninghe Damsté, J.S., 2003, Extremely high sea-surface temperatures at low latitudes during the middle Cretaceous as revealed by archaeal membrane lipids: Geology, v. 31, no. 12, p. 1069, doi: 10.1130/G19876.1.

Spicer, R.A., and Herman, A.B., 2010, The Late Cretaceous environment of the Arctic: A quantitative reassessment based on plant fossils: Palaeogeography Palaeoclimatology Palaeoecology, v. 295, no. 3-4, p. 423–442, doi: 10.1016/j.palaeo.2010.02.025.

Steuber, T., Rauch, M., Masse, J.P., Graaf, J., and Malkoč, M., 2005, Low-latitude seasonality of Cretaceous temperatures in warm and cold episodes: Nature, v. 437, no. 7063, p. 1341–1344, doi: 10.1038/nature04096.

Taylor, K.W.R., Huber, M., Hollis, C.J., Hernandez-Sanchez, M.T., and Pancost, R.D., 2013, Global and Planetary Change: Global and Planetary Change, v. 108, no. C, p. 158–174, doi: 10.1016/j.gloplacha.2013.06.011.

Upchurch, G.R., Otto-Bliesner, B.L., and Scotese, C., 1998, Vegetation–atmosphere interactions and their role in global warming during the latest Cretaceous: Philosophical Transactions of the Royal Society of London B, v. 353, p. 97-112.

Upchurch, G.R., Jr, Kiehl, J., Shields, C., Scherer, J., and Scotese, C., 2015, Latitudinal temperature gradients and high-latitude temperatures during the latest Cretaceous: Congruence of geologic data and climate models: Geology, v. 43, no. 8, p. 683–686, doi: 10.1130/G36802.1.

Vellekoop, J., Sluijs, A., Smit, J., Schouten, S., Weijers, J.W.H., Sinninghe Damste, J.S., and Brinkhuis, H., 2014, Rapid short-term cooling following the Chicxulub impact at the Cretaceous-Paleogene boundary: Proceedings of the National Academy of Sciences, v. 111, no. 21, p. 7537–7541, doi: 10.1073/pnas.1319253111.

Voigt, S., Wilmsen, M., Mortimore, R.N., and Voigt, T., 2003, Cenomanian palaeotemperatures derived from the oxygen isotopic composition of brachiopods and belemnites: evaluation of Cretaceous palaeotemperature proxies: International Journal of Earth Science. doi: 10.1007/s00531-003-0315-1.

Voigt, S., Gale, A.S., and Flögel, S., 2004, Midlatitude shelf seas in the Cenomanian-Turonian greenhouse world: Temperature evolution and North Atlantic circulation: Paleoceanography, v. 19, no. 4,, doi: 10.1029/2004PA001015.

Wilson, P.A., and Opdyke, B.N., 1996, Equatorial sea-surface temperatures for the Maastrichtian revealed through remarkable preservation of metastable carbonate: Geology, v. 24, no. 6, p. 555-558.

Zachos, J.C., Stott, L.D., and Lohmann, K.C., 1994, Evolution of early Cenozoic marine temperatures: Paleoceanography, v. 9, no. 2, p. 353-387.

Zakharov, Y.D., Popov, A.M., and Shigeta, Y., 2006, New Maastrichtian oxygen and carbon isotope record: additional evidence for warm low latitudes: Geosciences Journal, v. 10, no. 3, p. 347-367.

Zhou, J., Poulsen, C.J., pollard, D., and White, T.S., 2008, Simulation of modern and middle Cretaceous marine delta O-18 with an ocean-atmosphere general circulation model:

Paleoceanography, v. 23, no. 3, doi: 10.1029/2008PA001596.

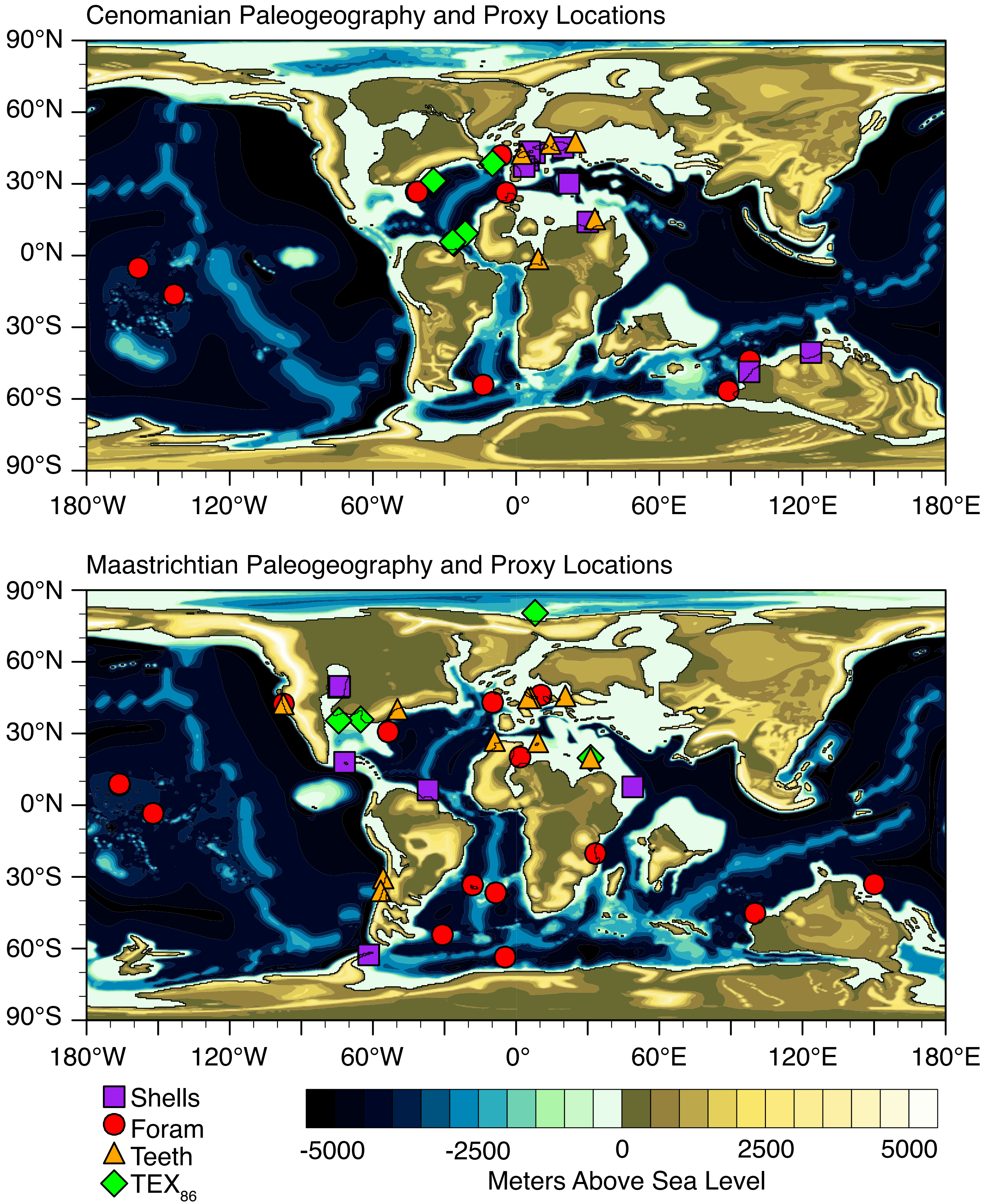
Cenomanian Paleogeography and Proxy Locations
90°N
60°N
30°N
0°N
30°S
60°S
90°S
180°W
120°W
60°W
0°
60°E
120°E
180°E
Maastrichtian Paleogeography and Proxy Locations
Shells
Foram
Teeth
TEX86
-5000
-2500
0
2500
5000
Meters Above Sea Level

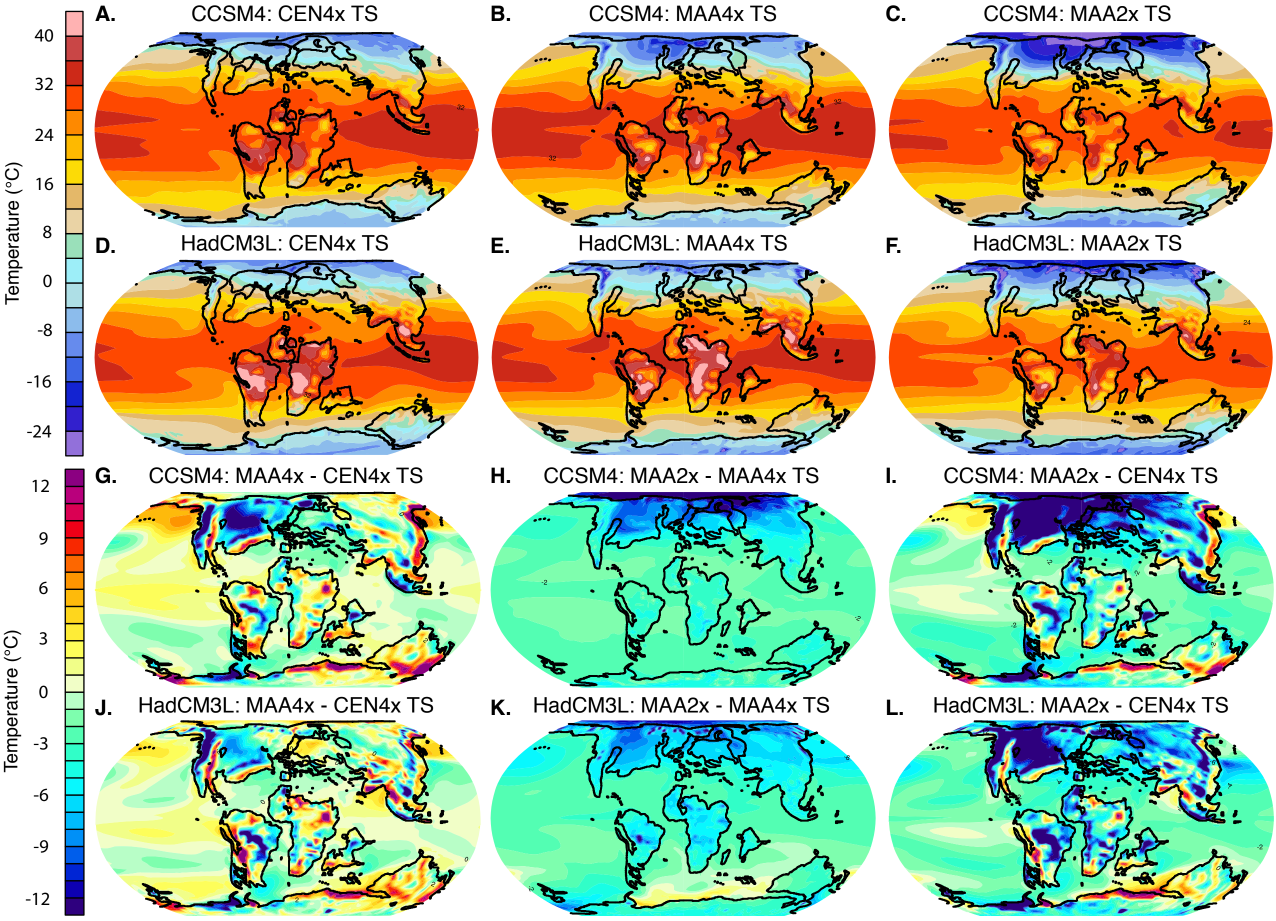

A. CCSM4: CEN4x TS
B. CCSM4: MAA4x TS
C. CCSM4: MAA2x TS
D. HadCM3L: CEN4x TS
E. HadCM3L: MAA4x TS
F. HadCM3L: MAA2x TS
G. CCSM4: MAA4x - CEN4x TS
H. CCSM4: MAA2x - MAA4x TS
I. CCSM4: MAA2x - CEN4x TS
J. HadCM3L: MAA4x - CEN4x TS
K. HadCM3L: MAA2x - MAA4x TS
L. HadCM3L: MAA2x - CEN4x TS
Temperature (°C)
40
32
24
16
8
0
-8
-16
-24
Temperature (°C)
12
9
6
3
0
-3
-6
-9
-12

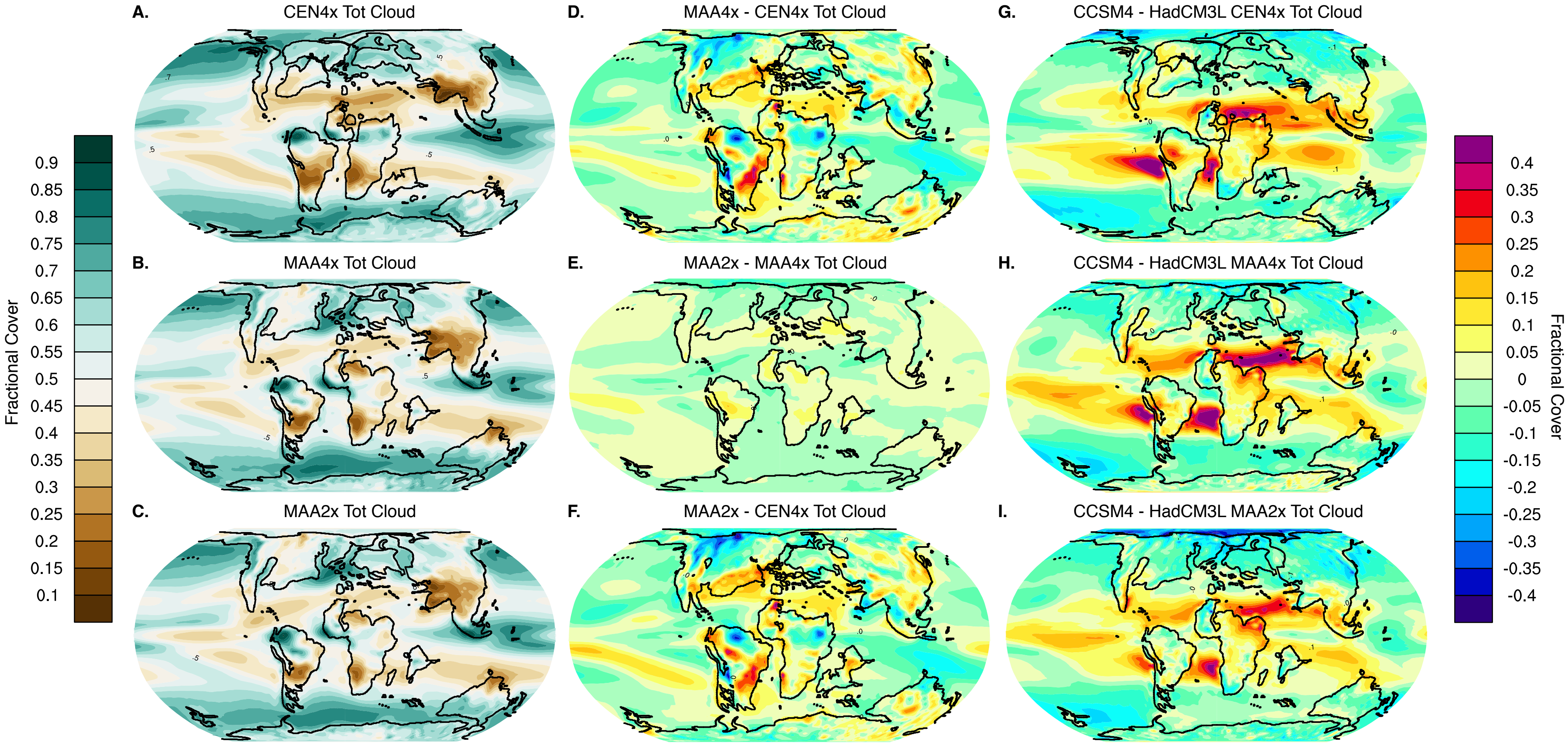

A.
CEN4x Tot Cloud
B.
MAA4x Tot Cloud
C.
MAA2x Tot Cloud
D.
MAA4x - CEN4x Tot Cloud
E.
MAA2x - MAA4x Tot Cloud
F.
MAA2x - CEN4x Tot Cloud
G.
CCSM4 - HadCM3L CEN4x Tot Cloud
H.
CCSM4 - HadCM3L MAA4x Tot Cloud
I.
CCSM4 - HadCM3L MAA2x Tot Cloud
Fractional Cover
0.9
0.85
0.8
0.75
0.7
0.65
0.6
0.55
0.5
0.45
0.4
0.35
0.3
0.25
0.2
0.15
0.1
Fractional Cover
0.4
0.35
0.3
0.25
0.2
0.15
0.1
0.05
0
-0.05
-0.1
-0.15
-0.2
-0.25
-0.3
-0.35
-0.4

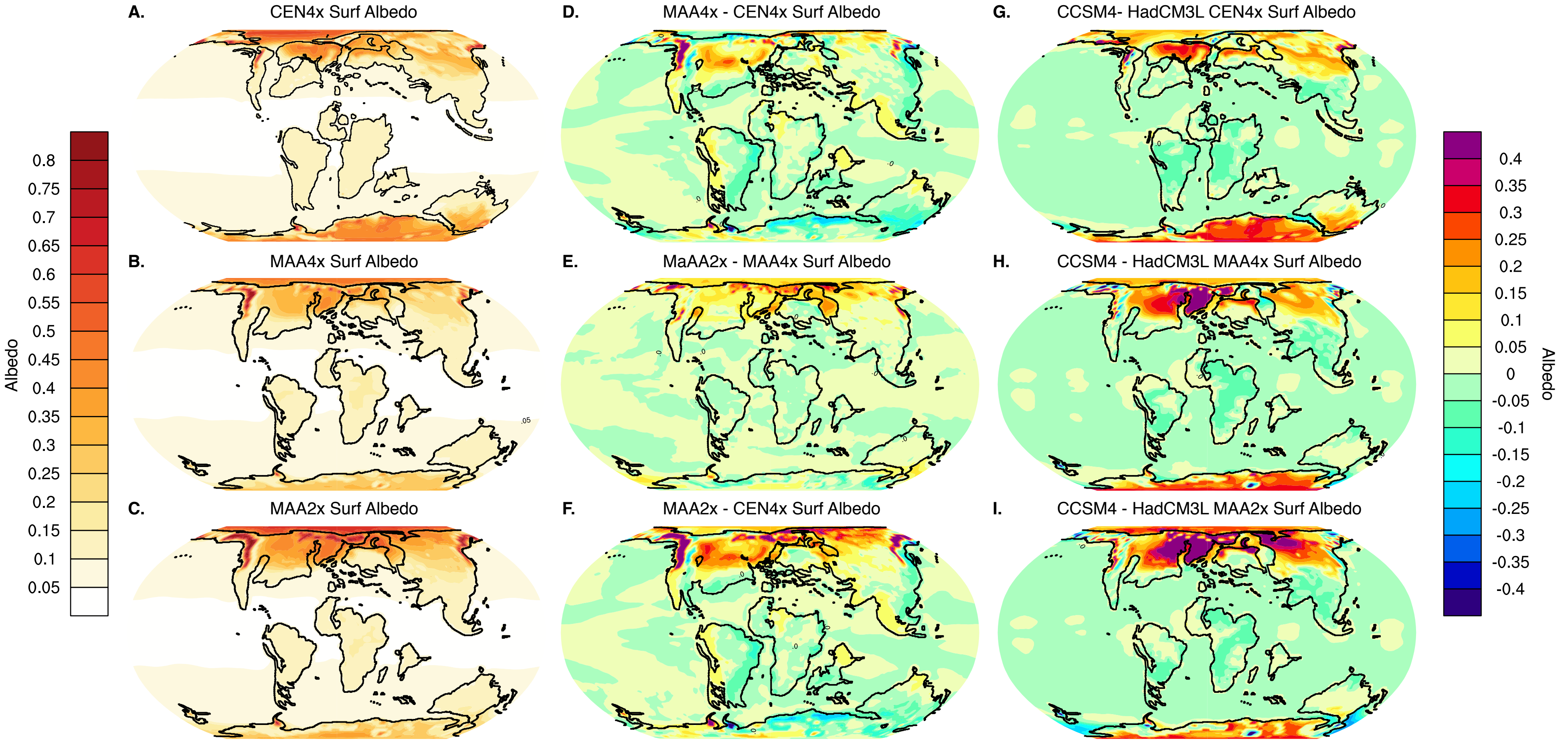

A.
CEN4x Surf Albedo
B.
MAA4x Surf Albedo
C.
MAA2x Surf Albedo
D.
MAA4x - CEN4x Surf Albedo
E.
MaAA2x - MAA4x Surf Albedo
F.
MAA2x - CEN4x Surf Albedo
G.
CCSM4- HadCM3L CEN4x Surf Albedo
H.
CCSM4 - HadCM3L MAA4x Surf Albedo
I.
CCSM4 - HadCM3L MAA2x Surf Albedo
Albedo
0.8
0.75
0.7
0.65
0.6
0.55
0.5
0.45
0.4
0.35
0.3
0.25
0.2
0.15
0.1
0.05
Albedo
0.4
0.35
0.3
0.25
0.2
0.15
0.1
0.05
0
-0.05
-0.1
-0.15
-0.2
-0.25
-0.3
-0.35
-0.4

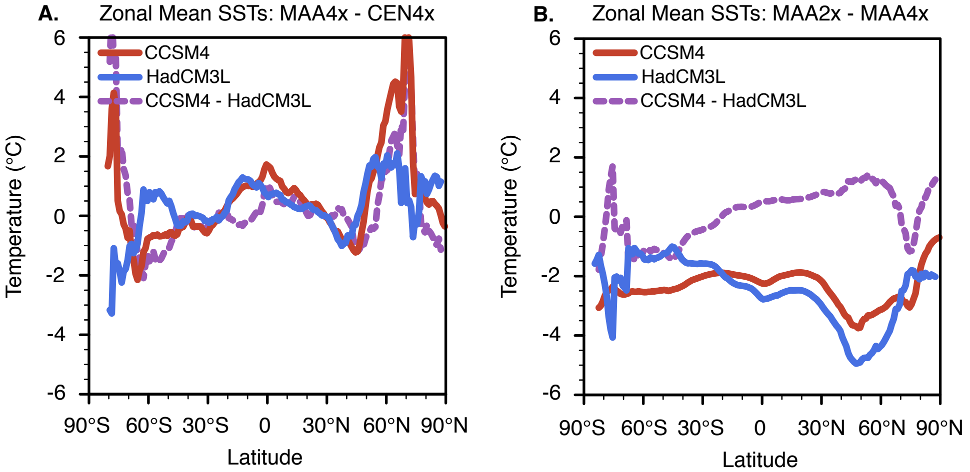

A.
Zonal Mean SSTs: MAA4x - CEN4x
B.
Zonal Mean SSTs: MAA2x - MAA4x
CCSM4
HadCM3L
CCSM4 - HadCM3L
Temperature (°C)
6
4
2
0
-2
-4
-6
90°S 60°S 30°S 0 30°N 60°N 90°N
Latitude

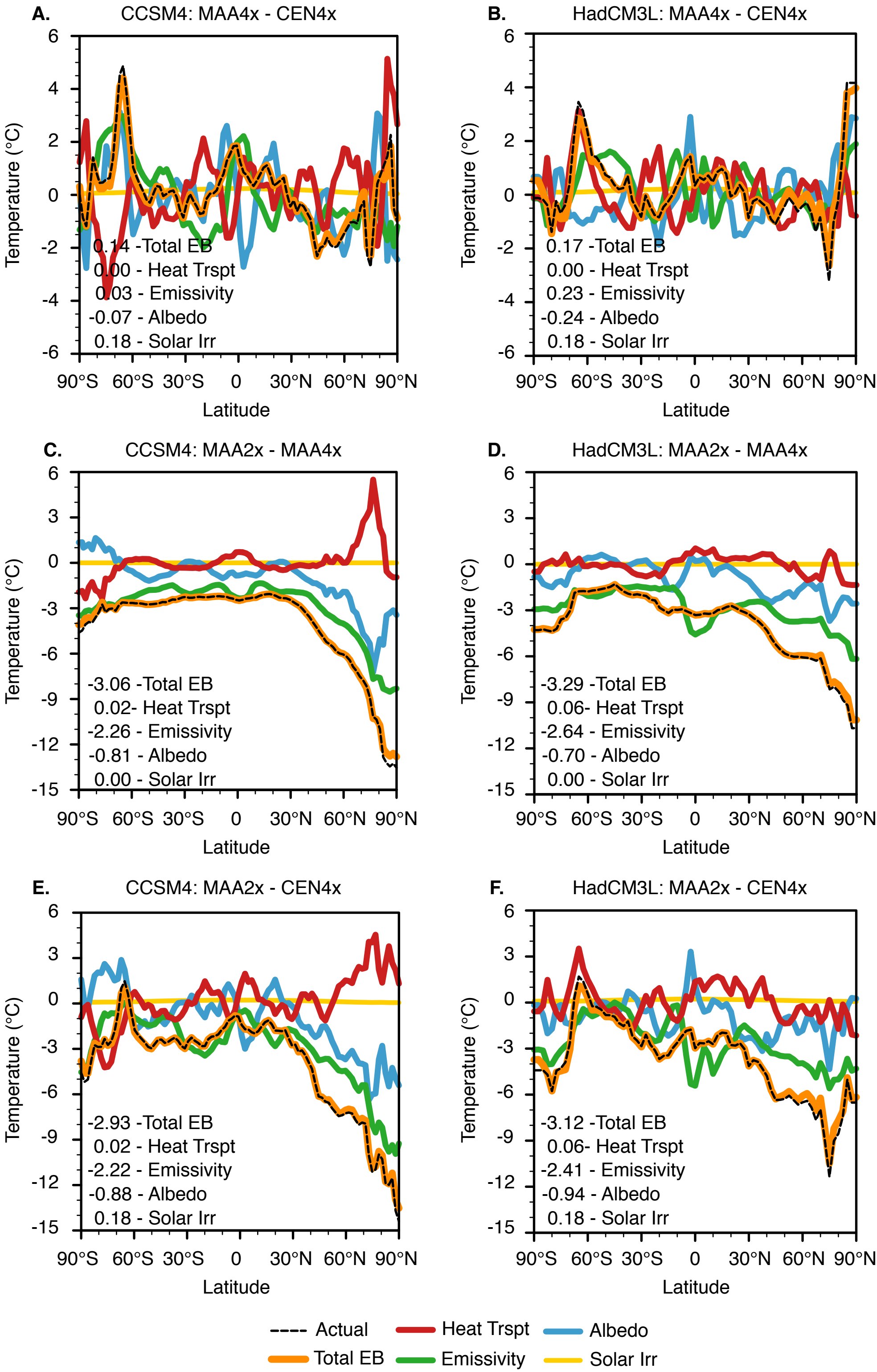

A.
CCSM4: MAA4x - CEN4x
0.14 -Total EB
0.00 - Heat Trspt
0.03 - Emissivity
-0.07 - Albedo
0.18 - Solar Irr
B.
HadCM3L: MAA4x - CEN4x
0.17 -Total EB
0.00 - Heat Trspt
0.23 - Emissivity
-0.24 - Albedo
0.18 - Solar Irr
C.
CCSM4: MAA2x - MAA4x
-3.06 -Total EB
0.02- Heat Trspt
-2.26 - Emissivity
-0.81 - Albedo
0.00 - Solar Irr
D.
HadCM3L: MAA2x - MAA4x
-3.29 -Total EB
0.06- Heat Trspt
-2.64 - Emissivity
-0.70 - Albedo
0.00 - Solar Irr
E.
CCSM4: MAA2x - CEN4x
-2.93 -Total EB
0.02 - Heat Trspt
-2.22 - Emissivity
-0.88 - Albedo
0.18 - Solar Irr
F.
HadCM3L: MAA2x - CEN4x
-3.12 -Total EB
0.06- Heat Trspt
-2.41 - Emissivity
-0.94 - Albedo
0.18 - Solar Irr
Temperature (°C)
Latitude
90°S 60°S 30°S 0 30°N 60°N 90°N
Actual
Heat Trspt
Albedo
Total EB
Emissivity
Solar Irr

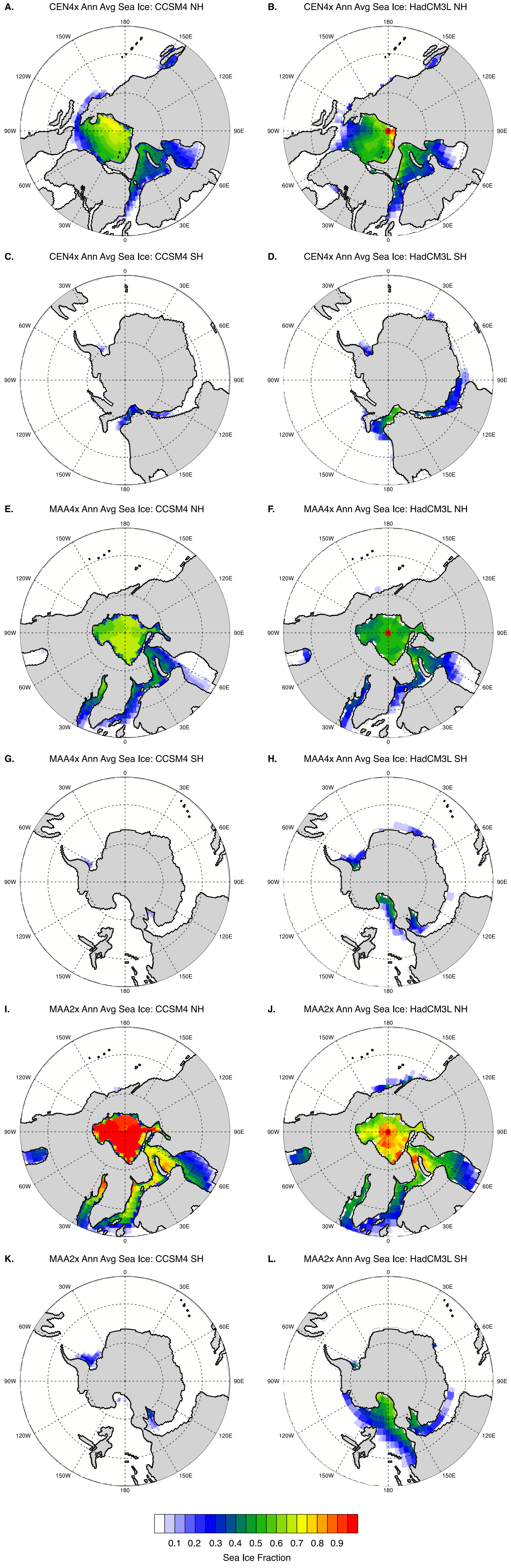

A.
CEN4x Ann Avg Sea Ice: CCSM4 NH
B.
CEN4x Ann Avg Sea Ice: HadCM3L NH
C.
CEN4x Ann Avg Sea Ice: CCSM4 SH
D.
CEN4x Ann Avg Sea Ice: HadCM3L SH
E.
MAA4x Ann Avg Sea Ice: CCSM4 NH
F.
MAA4x Ann Avg Sea Ice: HadCM3L NH
G.
MAA4x Ann Avg Sea Ice: CCSM4 SH
H.
MAA4x Ann Avg Sea Ice: HadCM3L SH
I.
MAA2x Ann Avg Sea Ice: CCSM4 NH
J.
MAA2x Ann Avg Sea Ice: HadCM3L NH
K.
MAA2x Ann Avg Sea Ice: CCSM4 SH
L.
MAA2x Ann Avg Sea Ice: HadCM3L SH
0.1 0.2 0.3 0.4 0.5 0.6 0.7 0.8 0.9
Sea Ice Fraction

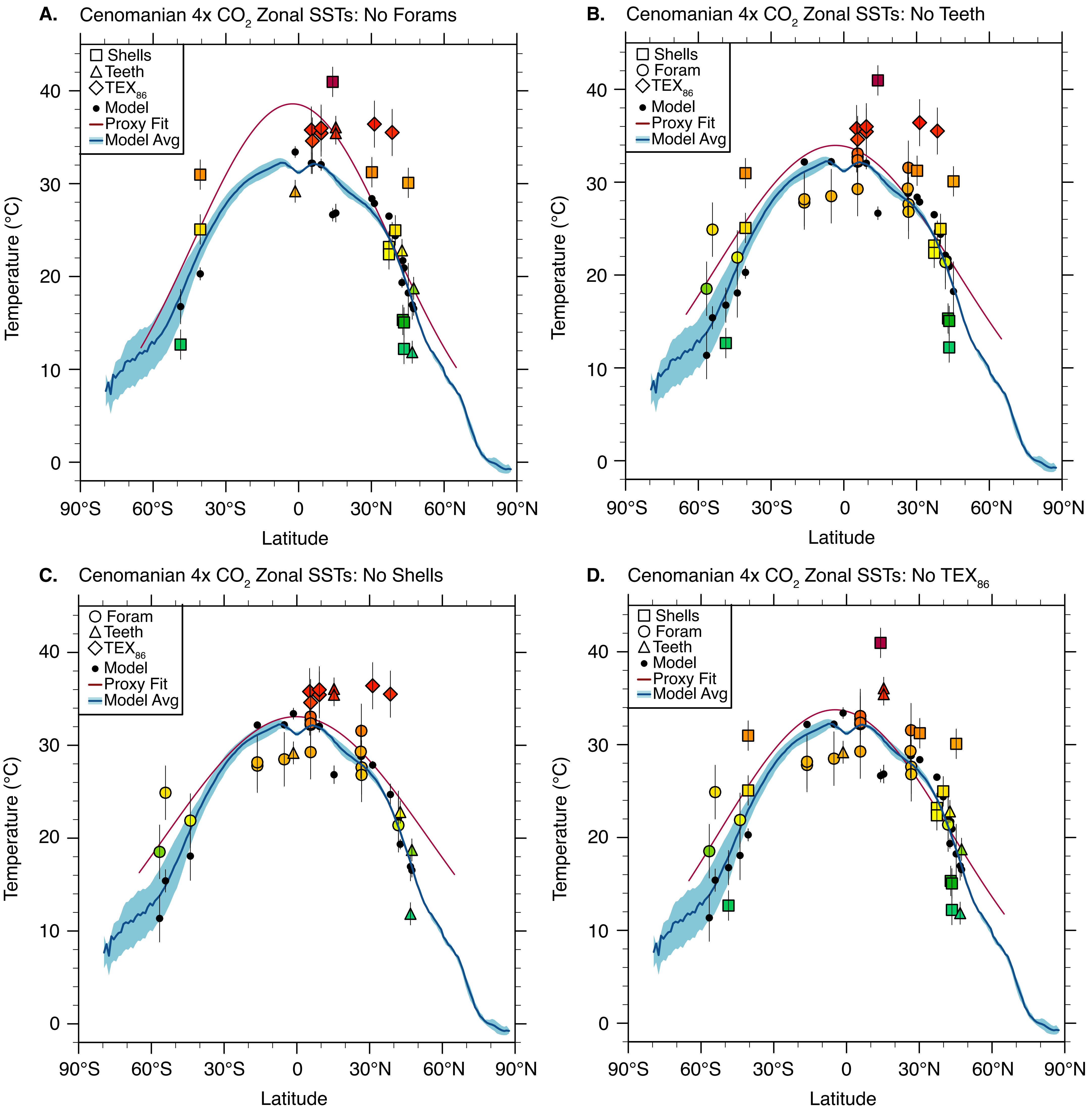

A.
Cenomanian 4x CO_2 Zonal SSTs: No Forams
Shells
Teeth
TEX_{86}
Model
Proxy Fit
Model Avg
Temperature (°C)
Latitude
90°S
60°S
30°S
0
30°N
60°N
90°N
B.
Cenomanian 4x CO_2 Zonal SSTs: No Teeth
Shells
Foram
TEX_{86}
Model
Proxy Fit
Model Avg
C.
Cenomanian 4x CO_2 Zonal SSTs: No Shells
Foram
Teeth
TEX_{86}
Model
Proxy Fit
Model Avg
D.
Cenomanian 4x CO_2 Zonal SSTs: No TEX_{86}
Shells
Foram
Teeth
Model
Proxy Fit
Model Avg

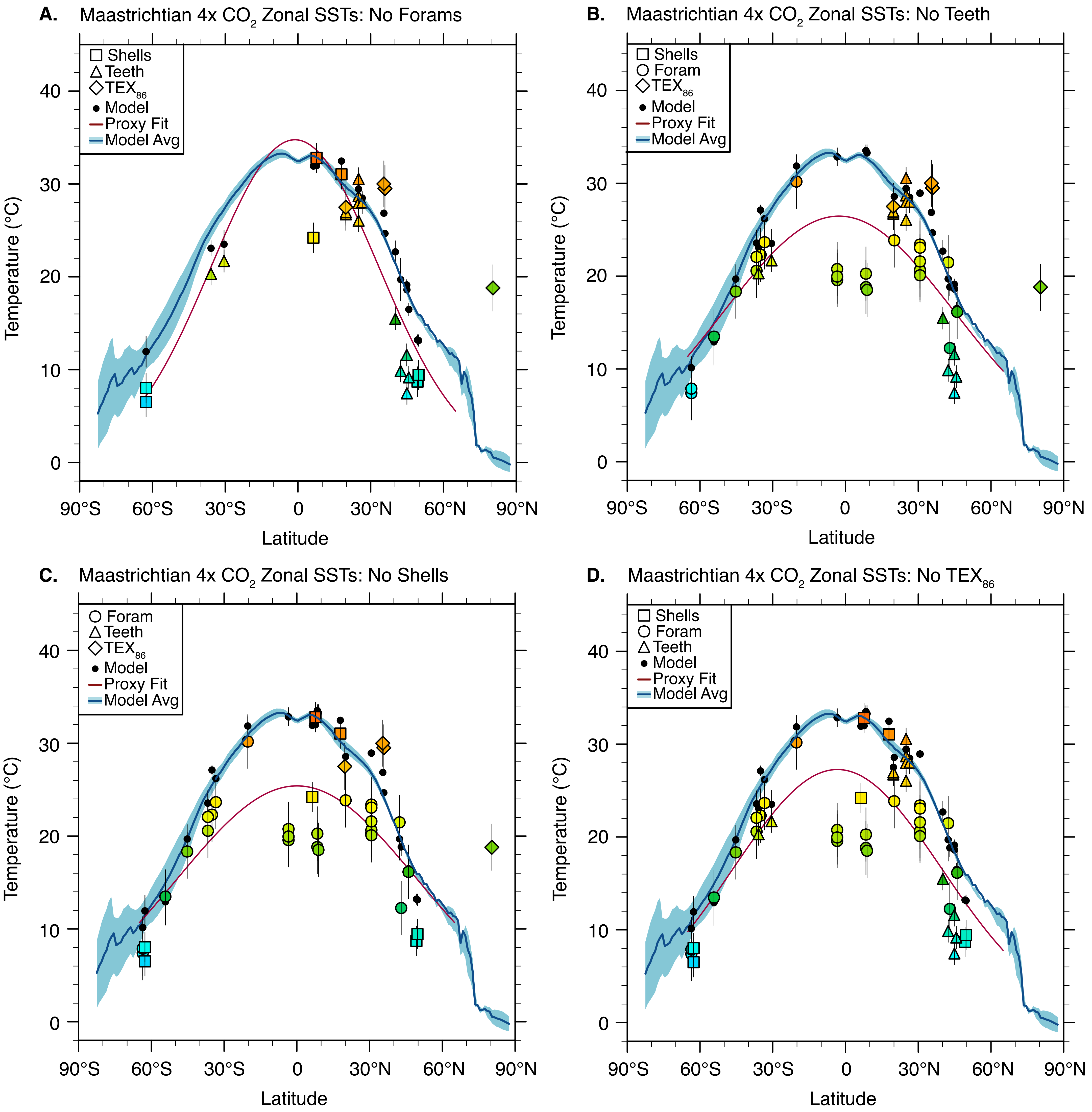

A. Maastrichtian 4x CO_2 Zonal SSTs: No Forams
Shells
Teeth
TEX_{86}
Model
Proxy Fit
Model Avg
Temperature (°C)
Latitude
B. Maastrichtian 4x CO_2 Zonal SSTs: No Teeth
Shells
Foram
TEX_{86}
Model
Proxy Fit
Model Avg
C. Maastrichtian 4x CO_2 Zonal SSTs: No Shells
Foram
Teeth
TEX_{86}
Model
Proxy Fit
Model Avg
D. Maastrichtian 4x CO_2 Zonal SSTs: No TEX_{86}
Shells
Foram
Teeth
Model
Proxy Fit
Model Avg
90°S
60°S
30°S
0
30°N
60°N
90°N
0
10
20
30
40

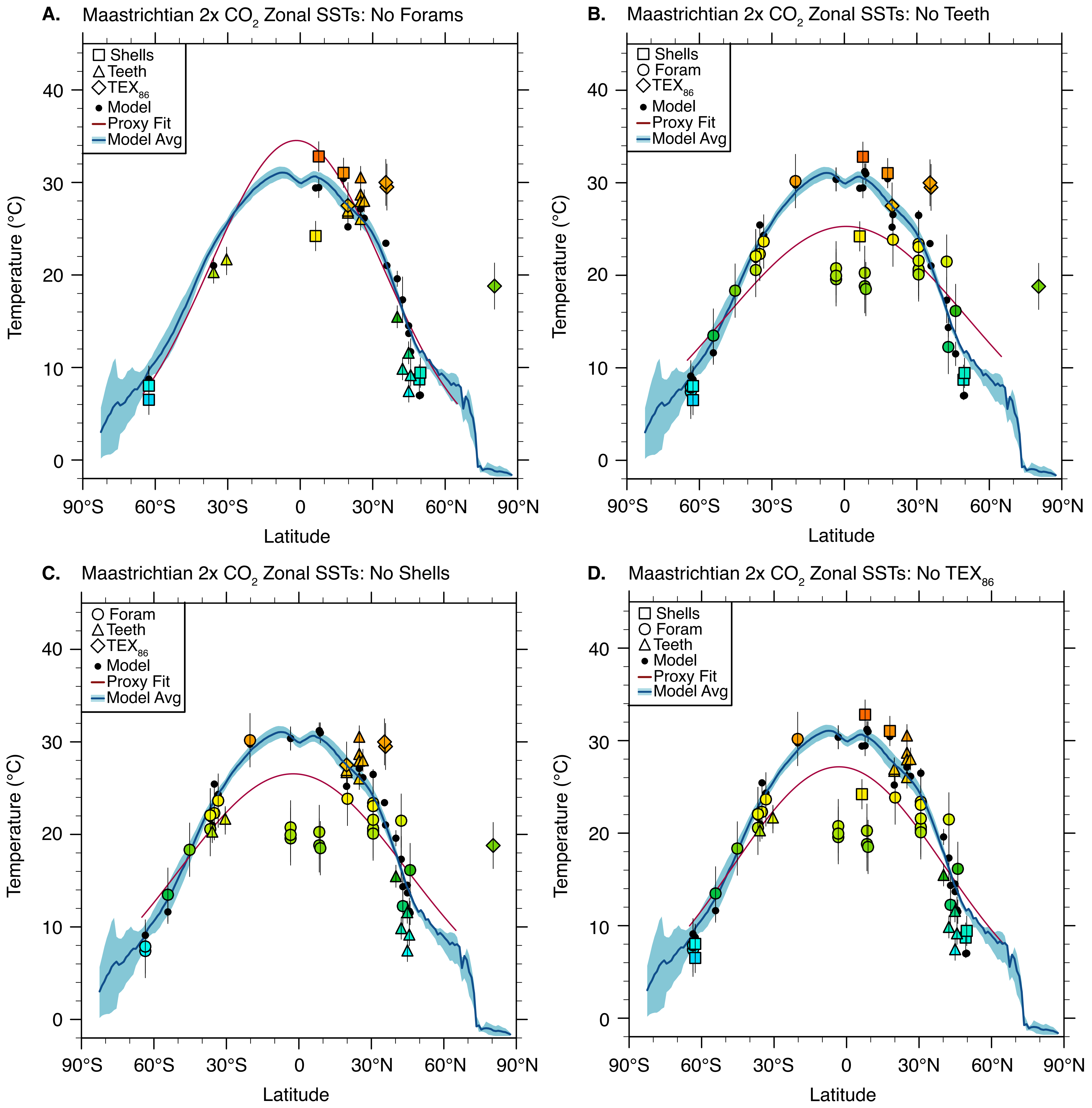
A. Maastrichtian 2x CO_2 Zonal SSTs: No Forams
Shells
Teeth
TEX_{86}
Model
Proxy Fit
Model Avg
B. Maastrichtian 2x CO_2 Zonal SSTs: No Teeth
Shells
Foram
TEX_{86}
Model
Proxy Fit
Model Avg
C. Maastrichtian 2x CO_2 Zonal SSTs: No Shells
Foram
Teeth
TEX_{86}
Model
Proxy Fit
Model Avg
D. Maastrichtian 2x CO_2 Zonal SSTs: No TEX_{86}
Shells
Foram
Teeth
Model
Proxy Fit
Model Avg
Temperature (°C)
Latitude
90°S 60°S 30°S 0 30°N 60°N 90°N
0 10 20 30 40

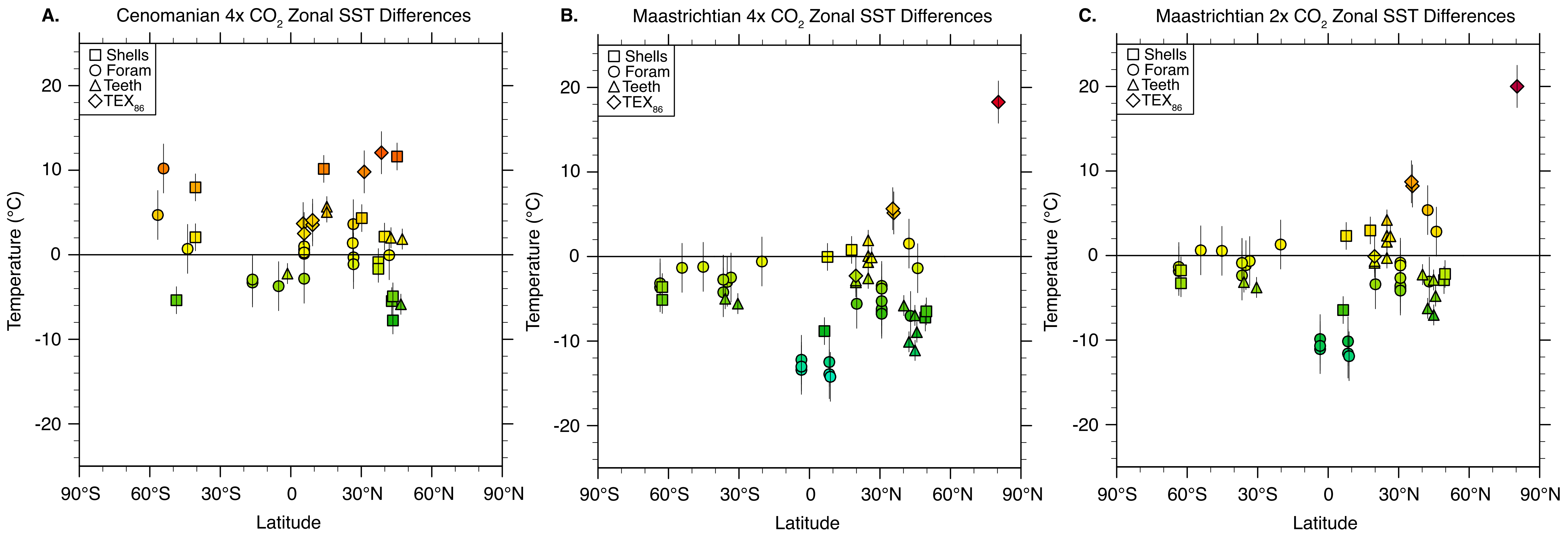

A.
Cenomanian 4x CO_2 Zonal SST Differences
B.
Maastrichtian 4x CO_2 Zonal SST Differences
C.
Maastrichtian 2x CO_2 Zonal SST Differences
Shells
Foram
Teeth
TEX_{86}
Temperature (°C)
20
10
0
-10
-20
90°S
60°S
30°S
0
30°N
60°N
90°N
Latitude